POLITECNICO DI MILANO

Facoltà di Ingegneria Industriale

Corso di Laurea Magistrale in Ingegneria Aeronautica

LiDAR Technology with Un-Frozen Turbulence for Wind Turbine Predictive Control

Relatore: Prof. Carlo Luigi BOTTASSO

Co-relatore: Ing. Carlo Emanuele Dionigi RIBOLDI

Tesi di Laurea di:

Leonardo TASCA Matr. 761763

Anno Accademico 2012 - 2013

Acknowledgements

I want to thank my dear family, my parents, my sister Ilaria, my cousins Giovanni and Emiliano, my uncles and my grandparents for their support and encouragement that accompanied me throughout my whole life. In particular I want to thank Anna Paola for her support and happiness, for the wonderful moments that we spent, and we will spend, together.

This work represents for me a great way to complete and to finish my studies at Politecnico di Milano, because it was a wonderfull research project exciting and fun. All of this would not have been possible without the opportunity given to me by Professor Carlo L. Bottasso to work with him and his research group. Then I want to thank him for this opportunity and for all his essential support. I also want to thank PhD. Carlo E.D. Riboldi for his strong support and to have been always available throughout my thesis work. Thank also to all research group Federico Gualdoni PhD. , Stefano Cacciola PhD. and Fillippo Campagnolo PhD for their friendliness.

I want to thank also all the Venice Friends, Seba, Riz, Marchetto and Mec and all those who have shared with me an unforgettable experience. I want to thank GP Nuoto Mira that for me it was like a second home.

Finally, and not least, I want to thank all friends who I met in Milan, Chicco, Perry, Sarti, Sapo, Jasmine and Salvatore; my roommates Michele, Luca e Fabio and all those who have made the university a better experience.

Abstract

The purpose of this work was to analyze the possibility of improving the use of LiDAR (Light Detection And Ranging) technology, as a sensor to provide the feed-forward information to the predictive controller, which scans a unfrozen wind field. It was also analyzed the improvements of predictive controls in comparison to a basic LQR controller. The predictive controls considered are Non Homogenus Linear Quadratic Regulator (NHLQR) and Receding Horizon Control (RHC). The new idea of LiDAR sensor, which scans an unfrozen wind field, arises to go beyond the limits imposed by the LiDAR used today, which it is based on Taylor Hypothesis of Frozen Turbulence. The unfrozen wind field is generated following the theory developed by Kirstensen, then to obtain that it is developed a empirical-mathematical model that allows to unfreeze the turbulence and a new wind generator, following Veers theory, that allows to elaborate a new more complex unfrozen wind filed history. Therefore the Frozen-LiDAR was updated with these mathematical models to perform unfrozen detection. To verify the performance of the Unfrozen-LiDAR in comparison to the Frozen-LiDAR as device of predictive controllers is used an aero-servo-elastic simulatior, CP-Lambda (Code for Performance, Loads and Aeroelasticity by Multi-Body Dynamic Analysis) developed by the Department of Aerospace Sciences and Technologies of Politecnico di Milano (DAST-Polimi). In this approach the wind turbine is modeled as a multi-body system, i.e., a complex model of interconnected flexible elements. In particular is useful to emphasize that the simulations were computed fulfilling the International Standard requirements. The results obtained are remarkable, the predictive controllers considered have significantly better performance, in some cases, than the controller reference considered, that it is the Linear Quadratic Regulator control (LQR). Instead the differences between simulations of predictive controls equipped with Unfrozen-LiDAR and Frozen-LiDAR are not significant.

Keywords: *Unfreezing, Turbulence, NHLQR, RHC, LiDAR, Longitudinal Coherence*

Sommario

Lo scopo di questo lavoro è stato quello di analizzare i possibili miglioramenti apportati mediante l'utilizzo di un sensore LiDAR (Linght Detection And Ranging), come strumento per fornire l'informazione predittiva ad un controllore in feed-forward, capace di rilevare la velocità del vento in un campo di vento definito scongelato. Inoltre sono stati analizzati i notevoli miglioramenti in termini assoluti apportati mediante l'utilizzo di controlli predittivi, quali Non Homogeneus Linear Qudratic Regulator (NHLQR) and Receding Horizon Control (RHC), in confronto ad un controllore di riferimento in feed-back, quale il Linear Quadratic Regulator (LQR). Il modello di LiDAR *scongelato*, ovvero un LiDAR capace di scansionare un campo di vento scongelato, è stato implementato prendendo in considerazione la teoria di turbolenza scongelata enunciata da Kirstensen, per ottenere un campo di vento scongelato a partire da una storia di vento di riferimento, in modo tale da rilassare l'ipotesi di Taylor (Ipotesi di turbolenza congelata) che è alla base dei LiDAR usati oggigiorno. Tale modello è stato prima verificato con un caso test e successivamente accorpato ad un generatore di vento turbolento scongelato, seguendo la teoria di Veers. Le simulazione delle turbine reali prese in considerazione, realizzate dal consorzio Innwind e dalla università nazionale di Kangwon, sono state attuate mediante un simulatore aero-servo-elastico virtuale multi corpo che prevede l'approssimazione del modello con elementi flessibili interconnessi, tale simulatore è stato sviluppato dal dipartimento di Scienze e Tecnologie Aerospaziali del Politecnico di Milano (DAST-Polimi), CP-Lambda (Code for Performance, Loads and Aeroelasticity by Multi-Body Dynamic Analysis). In particolare le simulazioni sono state eseguite seguendo i requisiti della Normativa. I risultati ottenuti sono notevoli. I controlli predittivi in termini di fatica e di qualità di potenza risultano essere ben più efficienti nei confronti dei controlli in feed-back. In particolare si può riscontrare come il LiDAR *scongelato* non contribuisce ad un sostanziale miglioramento in confronto al il LiDAR congelato, in termini di fatica, deviazione standard della potenza e deviazione standard della velocità angolare.

Parole Chiave: *Scongelamento, Turbolenza, NHLQR, RHC, LiDAR, Coerenza Longitudinale*

Riassunto

Introduzione

La ricerca in ambito energetico sta cercando di sviluppare nuove soluzioni per soddisfare il fabbisogno mondiale. Questa necessità nasce dal fatto che i maggiori protagonisti della produzione di energia sono caratterizzati da materiali non rinnovabili e altamente inquinanti, come petrolio, carbone, o le materie prime usate per produrre energia nucleare. Essendo non rinnovabili sono destinate a finire. Proprio in contrapposizione a questi metodi di trasformazione energetica, negli ultimi anni si stanno sviluppando diverse tecniche definite rinnovabili e soprattutto pulite, che sfruttano gli elementi naturali come il calore o il vento per produrre energia, ne sono un esempio fra tutti i pannelli solari e le turbine eoliche. Chiaramente queste tipologie di produzione energetica non possono soddisfare il fabbisogno mondiale, ne consegue che i vecchi metodi non possono essere accantonati. L'idea dei ricercatori, dunque, è quella di inserire le energie rinnovabili nell'equazione del mix energetico, che prevede oltre ad esse una sostanziale produzione di energia mediante i metodi tradizionali. Quello su cui si sta lavorando però è il peso che le rinnovabili hanno nell'equazione energetica. Ovviamente oggigiorno la produzione kW/h mediante energia rinnovabile ha un costo nettamente maggiore rispetto a quelle tradizionali, ed è proprio per questo che la ricerca ha come principale obiettivo la riduzione dei costi globali che riguardano i modelli di produzione energetica rinnovabile.

È in questo contesto che si inserisce il lavoro fatto per questa tesi. L'approccio è stato quello di valutare l'utilizzo di sensori di nuova generazione, con opportune modifiche, e capire se quest'ultimi possano garantire un effettivo vantaggio in termini di prestazione, quindi in termini di costo. Il sensore utilizzato è il LiDAR (Light Detection And Ranging), [9] [4] [5], che permette una previsione piuttosto accurata del campo di vento di fronte alla turbina. L'utilizzo di un sensore come questo prevede l'implementazione di strategie di controllo definite predittive, sviluppate di recente dal Dipartimento di Scienze e Tecnologie Aerospaziali del Politecnico Di Milano (DAST-Polimi), e in particolar modo dal gruppo di ricerca Poli-Wind. I controllori in questione sono il Non Homogenus Linear Quadratic Regulator (NHLQR) e Receding Horizon Control (RHC),[4], entrambi controllori in feed-forward, implementati in modo tale da poter sfruttare l'informazione di vento fornita dal LiDAR. Ad oggi un qualsiasi controllore installato su una turbina è caratterizzato da una strategia di controllo in

feed-back . L'informazione di vento utilizzata da quest'ultimi viene fornita da un anemometro posto dietro al rotore, in cima alla torre. Chiaramente è un informazione di vento ritardata in quanto il vento rilevato dall'anemometro ha già attraversato il rotore stesso. Il miglioramento imposto dal LiDAR è proprio quello di riuscire a rilevare l'informazione di vento di fronte alla turbina prima ancora che esso colpisca il rotore. Il problema principale del LiDAR ad oggi sviluppato è quello che l'informazione rilevata viene fornita al controllore senza considerare il fatto che nel tragitto che collega il punto di rilevamento e il rotore stesso, il vento evolve. Chiaramente il suo evolvere dipende dall'intensità turbolenta, dalla velocità media e dal profilo terrestre. Quindi i LiDAR ad oggi utilizzati possono definirsi LiDAR *congelati*, perché sono vincolati all'Ipotesi di Turbolenza Congelata di Taylor.

Il lavoro principale di questa tesi è stato quello di valutare la possibilità di scongelare la turbolenza e rilassare di conseguenza l'ipotesi di Taylor che caratterizza il LiDAR *congelato*. Il lavoro dunque prevede in prima analisi lo studio degli strumenti utilizzati, ovvero il LiDAR, i diversi controllori presi in considerazione e il simulatore areo-servo-eleastico utilizzato per simulare la turbina reale. Il secondo passo è stato quello di sviluppare il codice che permette di scongelare la turbolenza, verificarlo in un caso test, quindi implementare un generatore di vento scongelato e complesso, con griglia 2D in funzione del tempo. Questi codici implementati sono fondamentali per lo sviluppo di un LiDAR definibile *scongelato*, ovvero un LiDAR capace di scansionare un campo di moto scongelato. Una volta definito il simulatore virtuale che permette di rilevare il campo di vento scongelato di fronte ad esso si sono eseguite le simulazioni vere e proprie. Per simulare una turbina reale in un ambiente virtuale è stato utilizzato un codice sviluppato dal DAST-Polimi, ovvero CP-Lambda (Code for Performance, Loads and Aeroelasticity by Multi-Body Dynamic Analysis), [27] [28], un simulatore aero-servo-elastico dove la turbina viene rappresentata come un sistema multi corpo, quindi un modello complesso definito da elementi flessibili interconnessi. I controllori utilizzati sono come già definito i controllori predittivi NHLQR e RHC, inoltre per avere un confronto tra controllori in feedforward e in feedback è stato preso in considerazione un semplice Linear Quadratic Regulator Integral (LQR-Integral).

In particolare è utile enfatizzare come le simulazioni fatte si siano basate su modelli virtuali di turbine reali, ovvero la Turbina Kangwon 3MW, [34], e la Turbina Innwind 10MW, [35], con chiaramente dimensioni diverse anche dal punto di visto del rotore. Ne consegue che per segreto industriale i dati riportati in questa tesi sono tutti adimensionalizzati.

Campo di vento Scongelato

Il modello empirico matematico alla base dello scongelamento della turbolenza è stato sviluppato seguendo la teoria enunciata da Kirstensen nel suo principale articolo, [13]. La turbolenza può essere scongelata mediante il valore di coerenza longitudinale tra due punti uno considerato quello di riferimento, l'altro quello che rappresenta

l'evoluzione del vortice. Questo valore è fondamentale e viene definito a più riprese uguale ad una funzione esponenziale dove all'esponente abbiamo un fattore di decadimento, a, di ordine 10, moltiplicato per la frequenza del vortice, n, adimensionalizzata con D/U_0, dove D è la distanza tra il punto di riferimento e il punto da scongelare, e U_0 la velocità media della simulazione, [14] [15] [16] [20].

In particolare il sistema sperimentale installato da Kirstensen prevede due stazioni anemometriche in grado di rilevare il vortice. La stazione 1, è la stazione di riferimento mentre a distanza D da essa è presente la stazione 2 che rileva l'evolvere del vortice misurato precedentemente dalla stazione 1.

Si possono distinguere due modelli di scongelamento di turbolenza, uno basilare, determinato da un contributo di decadimento longitudinale, mentre il secondo viene definito in modo più complesso dalla probabilità di decadimento determinata dal prodotto di due contributi: quello longitudinale, e quello trasversale. Dunque nel secondo caso prendendo in considerazione la possibilità di una deriva laterale da parte del vortice.

In entrambi i modelli la coerenza puramente longitudinale viene determinata allo stesso modo, ovvero secondo la legge esponenziale sopra descritta. C'è la necessità di determinare la frequenza del vortice. Essa è legata all'inverso di una quantità fondamentale per lo scongelamento di un campo di moto, ovvero il tempo di riciclo del vortice, *Eddy Turnover Time*. Questo particolare tempo legato al decadimento della turbolenza viene definito come una legge di potenza legata all'energia cinetica turbolenta, e soprattutto dipendente dal range in frequenza del vortice (range inerziale o range energetico).

Per quanto riguarda il secondo modello ovvero quello con il doppio contributo, longitudinale e trasversale, bisogna definire la probabilità di deriva laterale quindi il contributo trasversale. Esso viene definito da Kirstensen nel suo articolo con un modello empirico matematico approssimato mediante diverse assunzioni. Le assunzioni che permettono di diminuire i parametri in gioco e semplificare il modello sono: il considerare stazionaria la velocità trasversale lagrangiana, considerare la varianza di quest'ultima uguale alla varianza della velocità longitudinale, mentre quella più importante definisce la diffusione trasversale come diffusione trasversale Gaussiana simmetrica assialmente. Inoltre essendo un modello principalmente empirico necessità di definire alcune caratteristiche della simulazione che permettono a seconda del caso di calcolare in modo più accurato la coerenza. Una di queste è la scelta del tipo di spettro turbolento in gioco, visto che per ogni modello di spettro corrisponde un parametro empirico diverso nella formula della coerenza. Lo spettro preso in considerazione in questo lavoro è lo spettro di Kaimal.

Ne consegue che il modello derivato dalla teoria di Kirstensen definisce un parametro di coerenza , che determina il decadimento di un determinato vortice in funzione della distanza tra i due anemometri, e in funzione della velocità media di trasporto del vortice. Tale sistema è stato verificato e collaudato con un caso test. Il caso test prevede la generazione di due serie temporali di vento, Eq. (3.18) e (3.19), una considerata passante per la stazione 1, mentre la seconda considerata come condizione all' *infinito*

del vento. Queste sono generate mediate una sommatoria che vede come termini lo spettro in funzione della frequenza moltiplicato per il coseno della frequenza adimenzionalizzata per il tempo della simulazione sommata ad un numero adimensionale che possiamo considerare come la fase del coseno, ϕ, e quindi come caratteristica distintiva tra le varie simulazioni di vento. La fase del coseno, ϕ può considerarsi come il seme distintivo del vento. Definita dunque la distanza D che separa la stazione di riferimento, 1, da quella *scongelata*, 2, possiamo creare la serie temporale di vento scongelato considerando la fase di tale serie, ϕ, uguale ad una funzione che vede come parametri le due fasi dei due venti di riferimento (stazione 1 ed infinto), quindi due semi diversi, e la radice quadrata della coerenza stessa, Eq. (3.25). Una volta calcolata la serie scongelata si è verificato la coerenza tra i tre venti generati.

Una volta verificata la bontà del modello di scongelamento si è voluto implementare da zero un codice che generasse un vento complesso costituito da una griglia 2D di valori in funzione del tempo, che avesse al suo interno il modello di scongelamento della turbolenza, in modo tale che, dato un vento di riferimento, si potesse generare la sua evoluzione ad una certa distanza dal punto in cui viene idealmente rilevato. Il vento di riferimento, in questo lavoro, è il vento visto dalla turbina, ovvero quello che effettivamente colpisce il rotore. Dunque con questo programma, definite due fasi da considerare come riferimento di vento *congelato*, un agente sulla turbina l'altro è la condizione all'infinito, si ha la possibilità di generare una terza storia di vento turbolento, da considerarsi *scongelato*. In particolare bisogna sottolineare il fatto che un vento turbolento è funzione dell'Intensità Turbolenta, che è stata scelta uguale al 16%, corrispondente alla turbolenza di tipo A (Normativa). L'intensità turbolenta definisce la deviazione standard della velocità longitudinale, mentre il modello e le dimensioni della turbina definiscono la scala di lunghezza integrale di turbolenza. Quindi una volta definiti questi parametri fondamentali per la ricostruzione dello spettro è stato sviluppato il programma che permette di generare un vento turbolento, che soddisfi le richieste della Normativa, seguendo la teoria di Veers, [23].

LiDAR

Lo scopo di questa tesi è capire i possibili vataggi nell'utilizzo di un LiDAR che scansioni un campo di vento scongelato da uno che scansioni un campo di vento congelato secondo l'ipotesi di Taylor. Per questo motivo vengo distinti nella seguente trattazione due tipi di LiDAR, uno scongelato e uno congelato, le operazioni eseguite da entrambi sono le stesse, cambiano però i campi di moto che cercano di rilevare. Il LiDAR definito *scongelato* si differenzia da quello *congelato* in quanto le informazione che utilizzano, gli input, sono diverse. Il LiDAR *congelato* può utilizzare la storia di vento temporale ottenuta mediante il codice open source TurbSim, come se stesse osservando una storia di vento spaziale, dove la terza dimensione non è più il tempo ma la distanza longitudinale tra il punto di rilevamento del LiDAR e la turbina, questo grazie alla già citata Ipotesi di Taylor. È proprio questa approssimazione che si sta cercando

di rilassare con il LiDAR *scongelato*. Prima di descrivere le informazioni necessarie per il LiDAR *scongelato* è utile definire le operazioni che il LiDAR, qualsiasi esso sia, attua.

Il LiDAR è un sensore ottico che viene abitualmente montato sulla gondola della turbina e che emette un fascio di luce, o un laser (LASAR), che attraversando l'aria viene riflesso dalle piccole particelle che vi sono sospese, come sabbia, piccole gocce d'acqua e polline. Poichè queste particelle vengono trasportate dal vento la loro velocità è una buona approssimazione di quella del vento stesso. Il sensore è in grado di focalizzarsi ad una certa distanza e fornire una serie di misurazioni ad una determinata frequenza. La strategia di scansionamento del LiDAR prevede la rivoluzione del laser stesso secondo uno schema predefinito, solitamente circolare, in modo tale da evidenziare un volume. L'output del LiDAR quindi rappresenta la media volumetrica tra tutte le velcità rilevate dal laser sul contorno del volume ottenuto. Come detto il laser è in grado di focalizzarsi in punti ad una certa distanza dalla turbina, chiamati appunto *Focus*. La velocità di questi particolari punti non viene rilevata dal LiDAR puntalmente, perchè in tal caso non fornirebbe una misurazione precisa, ma viene fornita mediando, secondo la funzione di Lorentz, la velocità di 101 punti scansionati in un rage di $+/-$ 30 m dal focus stesso. Ogni punto così determinato fa parte del perimetro descritto dalla rivoluzione del laser stesso. Quindi compiuta la prima media pesata con la funzione di Lorentz, la seconda viene eseguita tra tutti i punti che costituiscono lo schema di rivoluzione del laser, ottenendo così un unico valore per ogni distanza focale. Infine l'ultima media fornisce il valore di velocità mediata appunto tra i valori ottenuti in precedenza (uno per ogni focus). Di conseguenza l'informazione finale che il LiDAR fornisce è un valore di velocità per ogni istante di tempo.

Il LiDAR sviluppato dal gruppo di ricerca POLI-Wind è costituito da una frequenza di campionamento di 5 Hz, il che vuol dire che il laser impiega 0.2 secondi a spostarsi tra un punto di rilevamento dello schema ad un altro. Il percorso, quindi lo schema, definito dal LiDAR è circolare con 12 stop sulla circonferenza, il che significa che il LiDAR impiega 2.4 secondi a completare un giro. L'output del LiDAR fornisce un valore di velocità ogni 0.2 secondi, e non ogni 2.4 secondi. Questo significa che l'aggiornamento dello schema di rivoluzione del LiDAR viene eseguito ogni 0.2 secondi, di conseguenza tutti i punti di rilevamento dello schema vengono aggiornati ogni 2.4 secondi. Il numero di focus considerati sono 5, quindi vengo definite 5 distanze focali in funzione del diametro del rotore (da 0.5 diametri a 1.5 diametri). Ne consegue che i punti di campionamento per ottimizzare la pesatura alla Lorentz sono 505 per ogni stop sulla circonferenza. La dimensione della circonferenza descritta nell'ultima distanza focale è pari alla dimensione del rotore stesso.

Come accennato in precedenza l'input di un LiDAR *congelato* è radicalmente diverso da quello LiDAR *scongelato*, grazie all'ipotesi di Taylor. Un LiDAR *scongelato* deve necessariamente avere come input 505 storie di vento scongelate, una per ogni punto di rilevamento longitudinale lungo tutto il campo di moto di fronte alla turbina. Ne consegue che dato un vento di riferimento, ovvero il vento agente sul rotore, mediante i programmi precedentemente descritti si sono create le 505 storie di vento

scongelate una per ogni distanza dei punti di misura del LiDAR. Generate le storie di vento scongelato vengo dunque usate come input del LiDAR.

Risultati

Il sistema di simulazioni implementato è stato strutturato in modo tale da soddisfare la Normativa. Quindi ogni simulazione eseguita per ciascuna tipologia di controllo, è stata mediata con almeno 4 simulazioni riferite a 4 storie di vento diverse, in modo tale da ottenere un risultato statistico corretto. Le quattro storie di vento forniscono la base per le simulazioni riferite a controllori predittivi equipaggiati con LiDAR *scongelato*, in quanto queste storie forniscono il primo seme di turbolenza, quello che successivamente verrà considerato fisso. Per soddisfare la Normativa la simulazione riferita ad un qualsiasi controllore predittivo equipaggiato con un LiDAR *scongelato* necessita di essere mediata con i risultati di almeno 16 simulazioni, in quanto si deve considerare 4 simulazioni per il primo seme, e 4 simulazioni riferite al secondo seme per ciascun primo seme fissato in precedenza. Un riassunto delle simulazioni eseguite lo si può trovare in tabella 4.3.

I parametri che si utilizzano per attuare un confronto diretto tra i vari controlli sono: la fatica riferita al momento flettente agente sul fore-aft della torre, la deviazione standard della velocità angolare e la deviazione standard della potenza.

I risultati ottenuti sono notevoli, i controllori predittivi sono decisamente convenienti in termini di fatica e di deviazione standard della potenza, ma non solo, anche in termini di deviazione standard della velocità angolare si sono ottenuti dei risultati eccellenti. Questo andamento lo si può notare attraverso i risultati mostrati nelle figure 4.2, 4.4, 4.3, 4.5, 4.7, 4.6. In particolare si può evidenziare come la strategia di controllo in regione II limiti il vantaggio dei controlli predittivi in termini di fatica, questo perché la strategia di controllo in questa regione è determinata da una strategia a passo bloccato, quindi senza nessun tipo di attuazione attiva. Un altro elemento che vale la pena evidenziare è il grafico della deviazione standard della velocità angolare per la turbina dell'Innwind, 4.6(b). Questo grafico sembra evidenziare un problema da parte del controllo predittivo NHLQR, avendo in regione III dei valori di deviazione standard maggiori rispetto a quelli del normale LQR. Invece osservando il grafico 4.6(a) si può notare come tali differenze in termini percentuali siano davvero minime. Questo problema non è dipeso da un mal funzionamento in tale regione del controllore NHLQR, ma dal fatto che tale strategia di controllo non è stata completamente ottimizzata in termini dei guadagni del controllore. L'ottimizzazione della matrice dei guadagni è una procedura molto laboriosa in quanto i guadagni del controllore dipendendo da una particolare pesatura scelta dall'utente e che essendo riferita al vettore degli ingressi prevede diverse combinazioni. La dimensioni del vettore degli ingressi, è utile ricordare, è diversa da uno, trattandosi di controllori multi ingresso multi uscite (MIMO). Di conseguenza trovare l'esatta combinazione di pesi che permetta un perfetto quadro di risultati è molto complicato, ne sono un esempio i risultati ottenuti appunto con la

macchina di Innwind.

Un altro risultato importante da sottolineare è quello riguardante la potenza, infatti i controlli predittivi dimostrano di raggiungere una migliore *Power Quality*.

Infine va sottolineato il comportamento dei controlli predittivi equipaggiati con un LiDAR *scongelato*. I loro risultati sono comunque notevoli in confronto ad un semplice controllore in feedback. Al contrario se tali risultati li confrontiamo con quelli ottenuti mediante LiDAR *congelato*, quello che possiamo osservare è un andamento piuttosto simile, in alcuni casi identico. Questo implica che il scansionamento di un campo di vento scongelato rispetto un campo di vento congelato da parte del LiDAR non comporta sostanziali miglioramenti.

Conclusioni e Ulteriori Sviluppi

Lo scopo di questo lavoro è stato quello di analizzare la possibilità di eventuali miglioramenti nell'utilizzo di un LiDAR capace di scansionare un campo di vento scongelato, come sensore per fornire l'informazione in feed-forward al controllore di tipo predittivo. Inoltre sono stati verificati i notevoli miglioramenti indotti dall'utilizzo di controlli predittivo al posto di semplici controlli in feed-back. Come descritto nel *capitolo 3* il LiDAR definito scongelato neccessita come input un campo di vento scongelato. La teoria alla base del scongelamento di un campo di moto è stata sviluppata da Kirstensen, e avviene mediante un modello matematico che permette di scongelare la turbolenza dato come ingresso la velocità media del vento e la distanza tra il punto da scongelare e il punto di riferimento. Questo modello, inizialmente non legato al sensore LiDAR, è stato sviluppato negli anni '70 dello scorso secolo, dunque largamente verificato. È un modello semi-empirico ed è strettamente correlato al modello di turbolenza che si vuole scegliere, quindi tipo di spettro, intensità di turbolenza, e scala di lunghezza integrale di turbolenza. Il modello fornisce dunque un valore di coerenza in funzione della frequenza, questo valore è utile per determinare il *passaggio* da una storia di vento ad un'altra, determinando dunque un terzo vento definito appunto scongelato. Solo recentemente si è voluto potenziare il sensore LiDAR *congelato* con questo modello matematico rendendolo appunto *scongelato*, cioè in grado di rilevare un campo di vento scongelato. Questo perché si è sentita la necessità di migliorare l'informazione fornita al controllore predittivo nella speranza di migliorare ulteriormente le sue prestazioni. Questo in linea teorica dovrebbe essere vero, ciò però che si è verificato con questo lavoro è qualcosa di diverso.

Sono state confermate le ottime prestazioni dei controlli predittivi, verificandoli con turbine reali di diversa grandezza e produzione di energia. Si è compreso dunque che l'utilizzo dei controlli predittivi possa diminuire in modo significativo i costi che comportano la produzione e la manutenzione della macchina. Questo perché come ben si può notare dai grafici riportati nel *capitolo 4* la fatica riferita al carico agente sul fore-aft della torre si riduce sensibilmente rispetto ad un basilare controllo LQR-integral. Anche se entrambe le tipologie di controllo danno risultati più che vantaggiosi

in termini di deviazione standard della velocità angolare, il che sta a significare un pregio per entrambi i controllori, la deviazione standard della potenza è molto bassa per quanto riguarda un controllore predittivo, il che sta a significare una *Power Quality* decisamente migliore.

Per quanto riguarda invece il caso in cui si utilizzi un controllore predittivo equipaggiato di un LiDAR scongelato i risultati ottenuti sono comunque notevoli, nel senso che sono nettamente migliori rispetto ad un basilare LQR. Ci si aspettava però risultati migliori rispetto anche ad un controllo predittivo di tipo congelato. Ciò non è avvenuto, i risultati, che come già detto sono mediati tra 4 differenti simulazioni per soddisfare le richieste della normativa, sono pressoché identici a quelli ottenuti mediante simulazione congelata. Dunque non si è ottenuto un sensibile miglioramento. Questo perché proprio per la natura del modello matematico che scongela la turbolenza con i parametri in ingresso considerati, dipendenti dalla turbina e dall'intensità turbolenta, forniscono un output del LiDAR non così diverso dal modello congelato. Ciò è dipeso dal fatto che come sostenuto nel *capitolo 3* le distanze dei focus dalla turbina non sono così enormi rispetto alle scale di lunghezza integrali in gioco nel modello. Di conseguenza il parametro di decadimento della turbolenza non è così elevato da produrre due segnali LiDAR totalmente differenti. Inoltre si può anche sottolineare il fatto che le piccole variazione che sussistono tra un modello di LiDAR e l'altro in termini di output una volta lette dal controllore possono venir livellate. Questo perché il controllore predittivo in generale è stato costruito su un modello approssimato di conseguenza c'è il rischio che agisca come filtro rispetto ad alcune perturbazioni.

In conclusione il controllo predittivo è la direzione giusta per dare un contributo considerevole alla diminuzione dei costi che riguardano la turbina eolica. Per quanto riguarda il LiDAR scongelato, per il momento sembra non dare i risultati sperati, o comunque quel considerevole miglioramento che giustifichi il costo della simulazione rispetto ad un LiDAR congelato.

Per il momento uno sviluppo futuro sul LiDAR *scongelato* non è contemplato. Solo di recente si è iniziato a raccogliere i primi dati sperimentali, da campagne su turbine reali equipaggiate con un LiDAR, ciò comporterà sicuramente la possibilità di validare il codice di scongelamento della turbolenza e la verifica del modello semi-empirico. Nel momento in cui tale modello viene raffinato e nel caso in cui fornisca valori considerevolmente migliori rispetto ad un sensore che scansiona un campo di vento congelato esso potrà allora essere preso in considerazione.

Per quanto riguarda in generale il sensore LiDAR esso momentaneamente è stato applicato solo per controllori predittivi a passo collettivo, ciò ovviamente può essere esteso alle altre tipologie di controllore. Infatti prendendo in considerazione un controllore a passo individuale l'informazione del LiDAR così come viene calcolata ora non ha alcun valore. Ma potendo utilizzare una coppia di LiDAR o semplicemente cambiando la medie volumetriche che vengono attuate oggigiorno dal LiDAR si potrebbe fornire delle informazioni utili per un controllore a passo individuale. Un esempio delle potenzialità del LiDAR è quello di poter fornire delle velocità per settore, o di fornire in generale il *wind shear* orizzonatale e verticale, ovviamente cambiando

lo schema percorso durante il campionamento e le modalità di medie.

Un altro aspetto su cui si può lavorare è migliorare il processo di definizione della pesatura del controllo. Uno dei passaggi più impegnativi in termini di tempo è stato quello del settaggio appunto dei pesi in gioco per ottimizzare la matrice dei guadagni. Un progetto futuro potrebbe riguardare lo sviluppo di un codice di ottimizzazione di tali pesi, in modo tale da garantire dei buoni risultati in termini di tempo ragionevoli.

Contents

List of Figures

List of Tables

Chapter 1

Introduction

Nowadays the energetic resource is an important issue. The purpose of many universities is to revolutionize the idea of energy production. This goal arises due to a new environmentalist vision of mankind, that wants to reduce the heavy pollution that has today. Another good reason is that most types of energy production are not renewable. In fact both coal and oil are bound to end, as well as the raw material of the nuclear energy. So research is required to solve this issue. In this context is introduced the exploitation of natural forces to produce energy such as *Wind Power*. This kind of energy is called renewable, it's very important precisely because it's theoretically infinite and completely clean.

Renewable energy production has become very important in last few years, but not enough to satisfy the request. For this reason we need to develop a new concept of energy mix. We must change the equation of energy production and give more weight to renewable. To do this, it need to improve the efficiency of renewable energy production and aim to lower costs. As it can be seen from the document [2], the trend is just that.

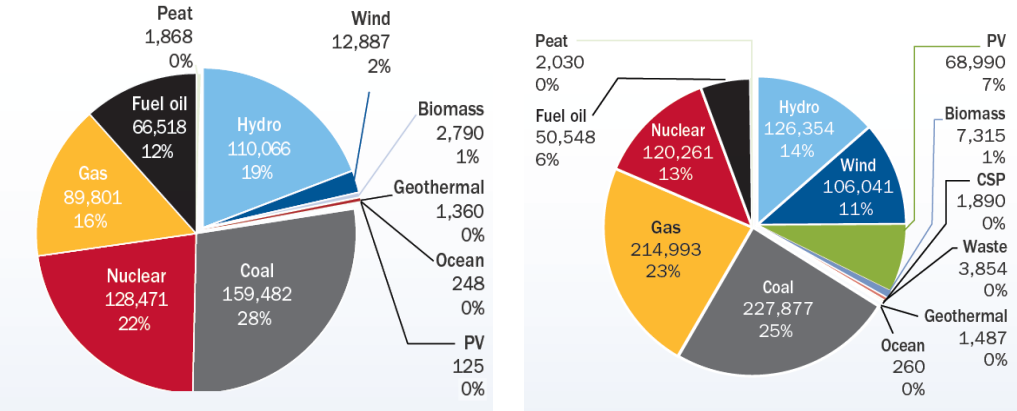

(a) *Europe Power Mix 2000* (b) *Europe Power Mix 2012*

Figure 1.1: Europe Power Mix

As it can be noticed in Figure 1.1, in Europe, wind power's share of total installed power capacity has increased five-fold since 2000; from 2.2% in 2000 to 11.4% in 2012. Over the same period, renewable capacity increased by 51%; from 22.5% in 2000 to 33.9% in 2012. In term of new installations there are three types of energy production that dominate the market: *Solar PV (37%)*, *Wind Power (26.5%)* and *Gas (23%)*. In Figure 1.2 (Data from document [2]) it can be noticed as old methods of energy production are at the edge of research and new investment.

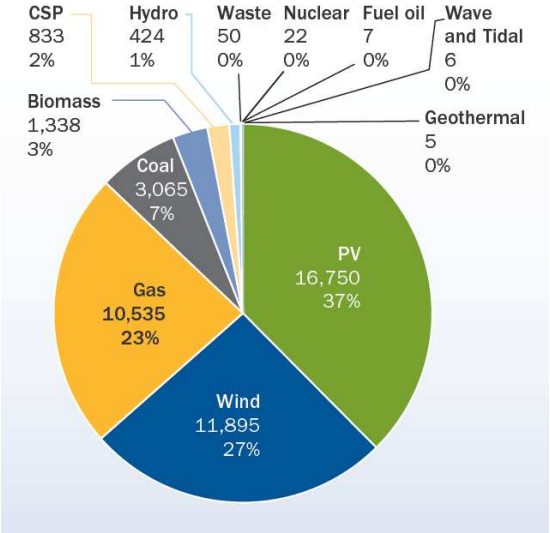

Figure 1.2: Share of new power capacity installation in Europe

It's almost 70% of all new installed capacity in EU is linked to renewable sources. Furthermore, it's the fifth year running that over 55% of all new power capacity in the EU is renewable. In particular 31 GW during 2012 have been installed (Figure 1.3).

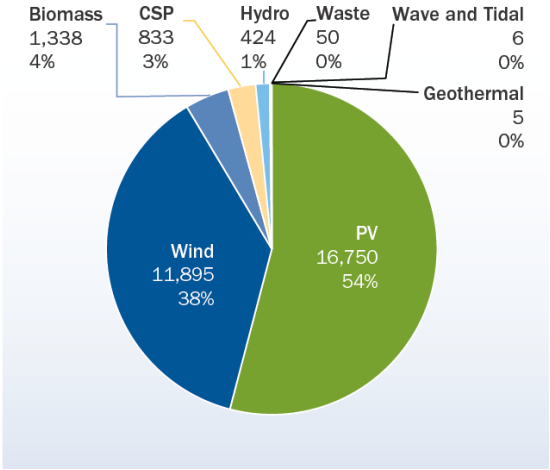

Figure 1.3: Share of new renewable power capacity installation in Europe

Not only Europe is interested to revolutionize this field, but it is a goal of many countries outside Europe. China and United State of America are the most active countries in this regard, as it can be shown in Figure 1.4

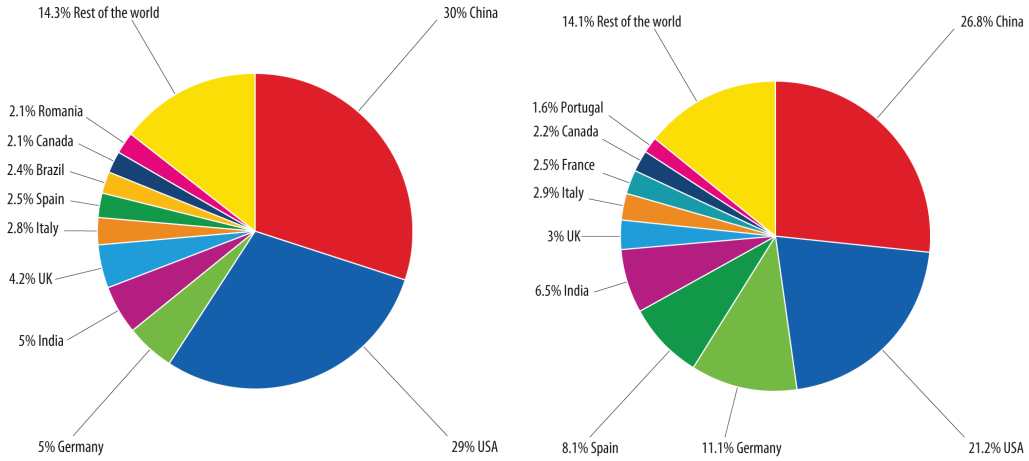

(a) *Top 10 new installed capacity in 2012* (b) *Top 10 new cumulative capacity in 2012*

Figure 1.4: Top 10 new installed and cumulative capacity in 2012

It's interesting to notice that China is one of the major countries that installed more MW of wind turbine, data from [1]. Though in 2009 this country seems to hasn't reached adequate level of energetic mix, Figure 1.5 (data from document [3]). In facts, the energy is produced from coal still has a primary role.

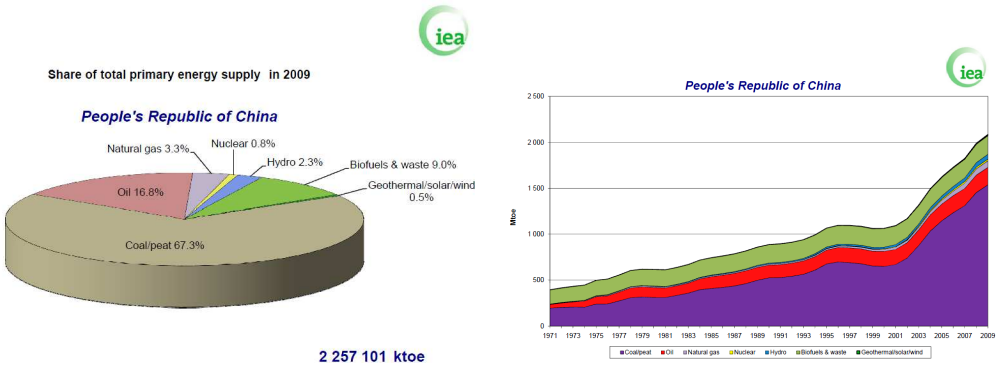

(a) *Share of total primary energy supply in 2009* (b) *Energy production from 1971 to 2009*

Figure 1.5: China statistic data of energy production in 2009

After the analysis of these data, it is important to emphasize that the investment on renewable energy is steadily increasing. Primary purpose of Research centers, universities, and energy companies is the continuous improvement of this technology, thus giving a primary role to renewable in the energy mix.

1.1 Wind Power

The wind power is the new way to covert energy in the last thirty years, and most important is one of new so-called renewable and clean energy. This kind of energy is very important because it does not produce greenhouse gases during operations, unlike energy linked to fossil fuels and oil. There are pollutant gases emissions only in machine production phase. Then during machine operating life it is produced clean electric power by a natural event: *Wind*. One of the defects that are associated to production energy through Wind Power is linked to wind turbines size. The landscape pollution is relevant, but is not different with whatever power station (hydroelectric, coal and nuclear power plant). However at the end of wind turbine operating life it is possible to remove the device and the landscape returns as it was before. This is not the case when traditional plants are removed

Exploitation of the wind power is not a XXI century discovery, in fact windmills have been exploited for more than two thousand years. Clearly the windmills role was totally different in comparison to modern wind turbine. They were less efficient, and in particular they produced mechanical energy and did not storage electric power. Only with modern era and its technology the windmills idea is evolved towards the wind turbine concept.

(a) *Windmill* (b) *Wind Turbine*

Figure 1.6: Types of Exploitation of Wind Power

This exponential growth of efficiency, due to an increasing interest by research centers, led wind energy to a more central role. During 2012, 12744 MW of wind power were installed across the Europe, of which 11895 MW were in the Europe Union (EU). Among its countries, the largest effort has been made by Germany (2415 MW), followed by UK and Italy, as it can be noticed in Figure 1.7 (data from document [2]).

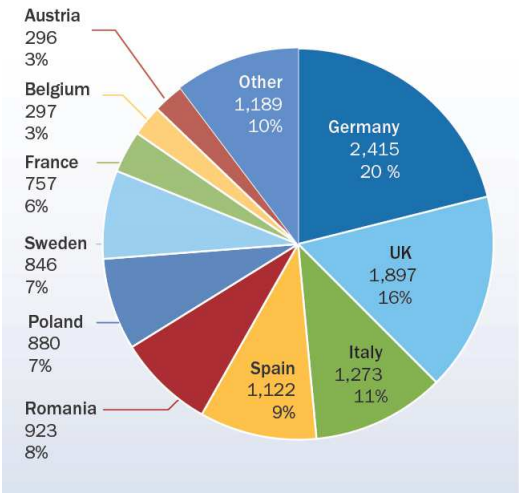

Figure 1.7: EU member state market shares for new capacity installed during 2012 in MW

To understand the weight of wind power it is interesting to observe that the wind capacity installed at end 2012 will, in a normal wind year, produce 231 TWh of electricity, that value representing 7% of the EU's gross final consumption. Denmark is the most virtuous country (Figure 1.8), which is occasionally able to meets its internal demand with only wind power.

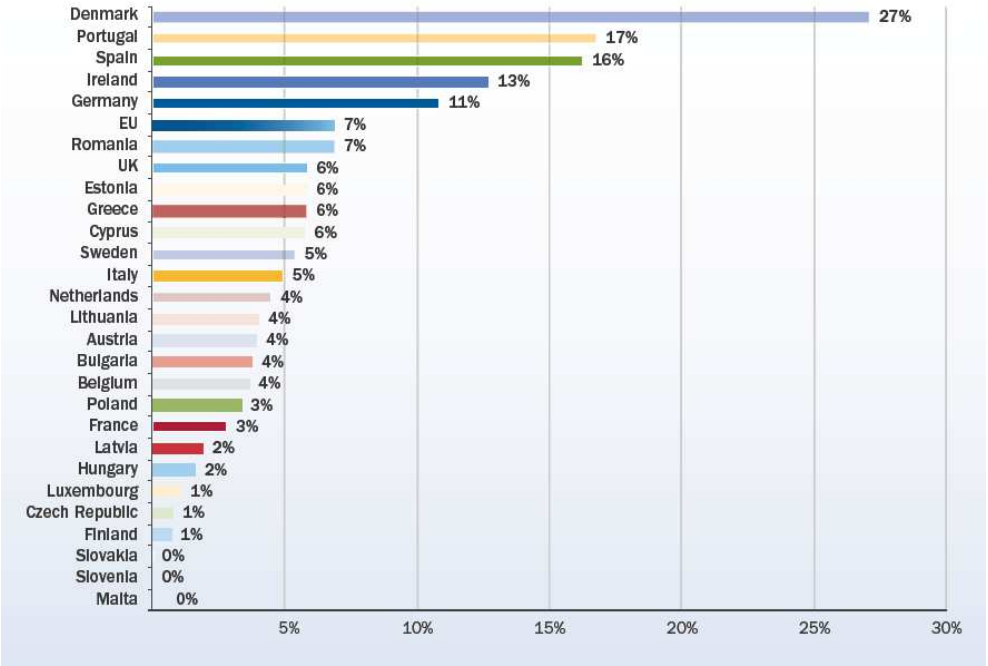

Figure 1.8: Wind power shear of total electricity consumption in EU and in member states

It's important to emphasize that only certain areas can be protagonists for this new frontier of energy production. In facts, the installation of wind turbine, or the design of wind farm, are closely linked to the presence on territory of high wind indices. This reason, combined with internal politics requirements moved the interest towards off-shore turbines. Because the annual wind presence is most relevant and because they are considered less pollutants to an environmental point of view.

1.2 Contributions of the present thesis

The purpose of this research is to improve the role of wind power in the energetic mix equation. To do that the main aim is to reduce the costs of wind energy. In particular there are three different types of cost: *maintenance costs*, *production costs* and *power cost* that depends on conversion efficiency of machine. In practical terms some performance indexes have been selected which are strictly bound to these cost components, like for instance the Fore-aft load, M_y (Figure 1.9), the standard deviation of power and the standard deviation of angular velocity. The first has an impact on the design and production cost of the tower, while the others are relevant under the power quality profile. Control laws are pivotal in driving this indexes, and hence it makes sense study sophisticated control strategies able to improve these indexes.

We have analyzed the possible advantages of using predictive control systems, and possible solutions to improve them. Nowadays all installed turbines are provided with a simple feed-back controller and this implies that the real control system is usually rather basic and underperforming on the quantities of interest. The greatest efforts in this area are concerned with a virtual development of new control techniques, which allow to reduce forces imposed on the turbine. This is possible thanks to the presence of virtual environments developed by different research centers that allow a realistic simulation, such as *Cp-Lambda* [27] [28] [8], *Bladed* [29], *FAST* [30]. In particular, recent works are addressed to innovative wind turbine control architectures able to treat a information about the incoming wind [4]. The latter is provided by the technology of a new sensor: the LiDAR (Light Detection And Ranging). A measure of the wind ahead of the rotor for each time instant is obtained by LiDAR with a volumetric mean of the wind field as will be explained in later chapters.

The a particular averaging action carried out by the real LiDAR sensor on the local wind speed of the free stream has a impact on the behavior of any predictive control laws. To suitably assess the performance of LiDAR and control assembly in simulation environment, it is necessary a virtual model of the LiDAR sensor. Today the majority of the existing LiDAR simulator is based on Taylor's frozen turbulence hypothesis.

The most important contribution of this work is to improve the information obtained by LiDAR sensor. Nowadays LiDAR technology is the state of the art of the predictive control, and it provides a frozen velocity input to the controller. It detects a set of wind grids in front of the turbine at specified distances, and it provides the average information without considering the fact that it will not be the same which will

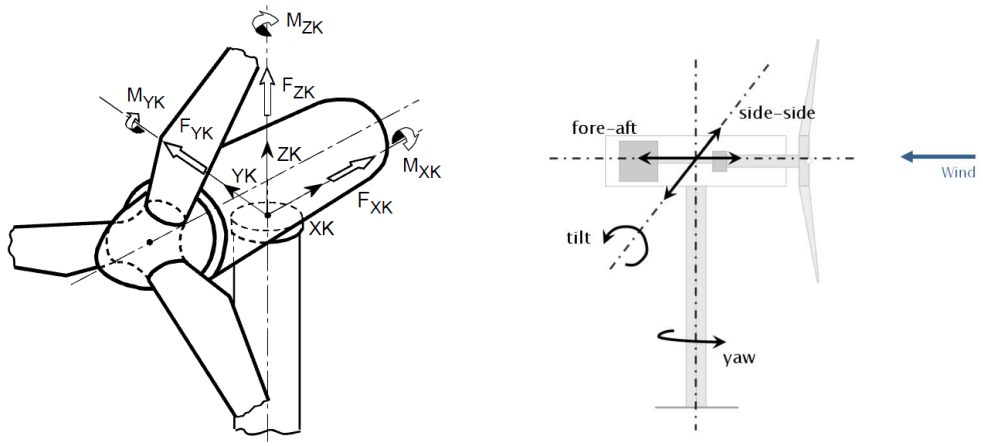

(a) *Skecth of tower coordinate system and the moments acting on tower*

(b) *Sketch of the main rigid movements of the system*

Figure 1.9: Sketch of tower coordinate system, its main rigid movements and moments acting on the tower

hit the turbine. Therefore recent works to setting up a model that allows to unfreeze the turbulence and to investigate the *exact* flow filed. The work is inserted in this research context. A new LIDAR simulator is developed considering interface with the available controller, this sensor is able to detect an unfrozen wind field in front of the turbine, the differences from the previous model do not concern the LiDAR operations but only the input that needs to detect an unfrozen wind field. In the following will be considered *Unfrozen LiDAR*, a LiDAR able to detect an unfrozen wind field, instead a *Frozen LiDAR* a LiDAR based on Taylor Hypothesis then able to detect a frozen wind field. For this purpose a new wind model generator is implemented, that it is able to unfreeze the turbulence. Then the frozen LiDAR model is reviewed and improved. In particular the implementation aspect has a fundamental role, because a model able to unfreeze the turbulence, may present numerical issues in terms of time simulation and data storage. In last chapter a full comparison between several control strategies working in conjunction with frozen or unfrozen turbulence is presented.

For completeness the study is carried out on two turbines of completely different sizes. One is the *Kangwon*, 3MW turbine with rotor diameter of 93 m, and the other is the Inwind machine, 10MW turbine with rotor diameter of 180 m. Afterwards the results are compared. Clearly the results reported here in will be dimensionless as they relate to real machines for which the design data are covered by industrial secrecy.

1.3 Outline

This work is developed in three phases:

- *Chapter 2:* In this chapter there is an exhaustive description of main characteristics of available tools and devices, in particular the state of the art of wind turbines, their characteristics, their different controllers and LiDAR sensors, then the description of the simulation software. The purpose of this section is to emphasize the difference between a feed-back and a feed-forward controller, because this is considered to be useful for the understanding of the work done.

- *Chapter 3:* This is the core of the research work. In this chapter there is a detailed description of different unfrozen turbulence models and how they are implemented and how they are included in the overall research work of the Department of Aerospace Sciences and Technologies of Politecnico di Milano (DAST-Polimi). Once the models are described, it follows a description of how they modified the turbulent wind generated and how a new turbulent wind generator is implemented, associating it with a code that complies with the requirements, *TurbSim* [25]. The last section of this chapter is centered on the explanation of the implementation aspects to ensure reasonable efficiency, in term of simulation time and data storage.

- *Chapter 4:* This chapter focuses on a description of simulations performed and on the comparison between their results. In particular there are some details of the wind turbines that we use.

Chapter 2

Wind Turbine

A wind turbine is a plant able to extract power from wind and transform it into electric power. The distinction between different types of wind turbine depends on how it work to extract wind power. There are mainly two types of machines that are distinguished by the direction of the rotation axis of the main rotor:

- *Horizontal-axis:* This type of machine can reach larger size and produces a greater amount of power. As it can be noted in Figure 2.1, the electric power, that can be extracted from turbulent wind, depends directly on the size of the turbine. Nowadays the largest wind turbine installed is a 7.5 MW turbine, having a rotor diameter of 126 m.
- *Vertical-axis:* This type of machine is less bulky, and usually smaller than a horizontal-axis wind turbine. Its typical feature is that it can be installed in sites where the wind direction is unstable and unknown. The main problem is that it produces less electrical power than a typical horizontal-axis wind turbine.

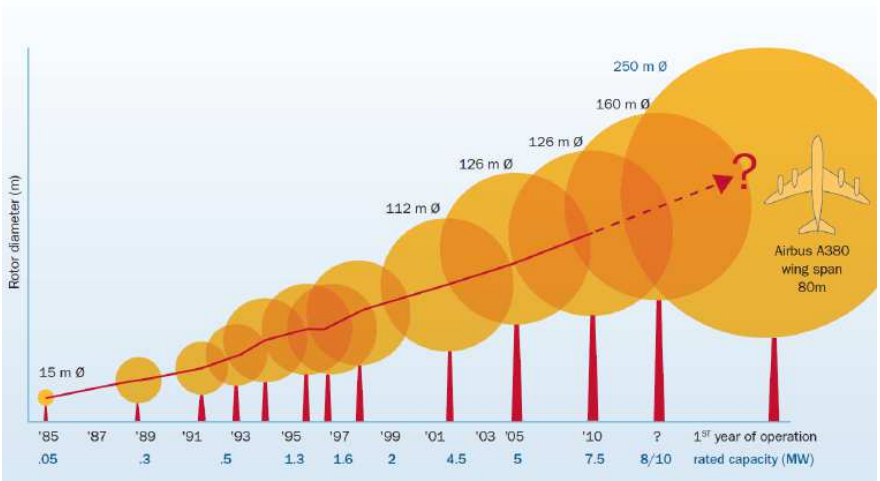

Figure 2.1: Comparison between size and power produced by wind turbine

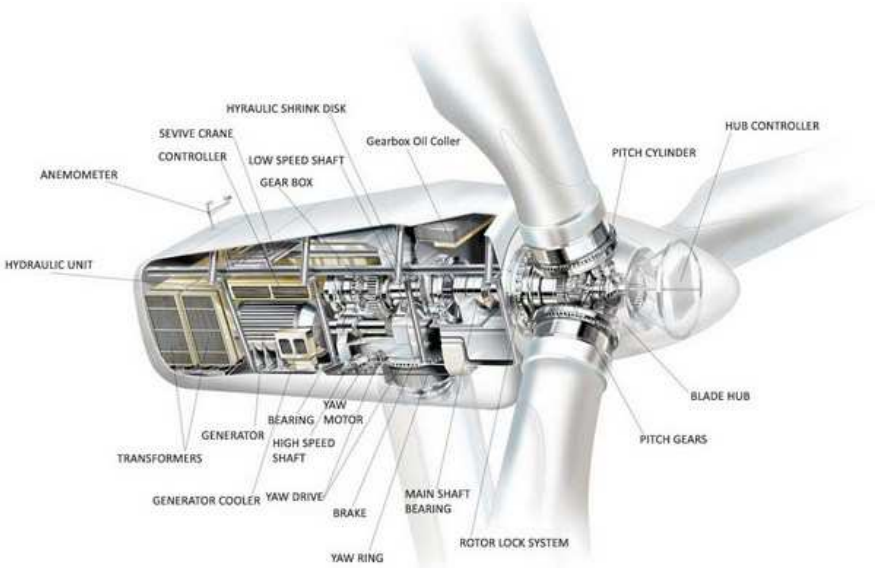

Figure 2.2: Sketch of upwind horizontal axis wind turbine components

2.1 General aspects

This work is concerned on horizontal-axis wind turbines, which, in a typical configuration show a three bladed rotor connected to the hub. Usually blades are constructed of carbon or glass fiber. The weight of main rotor, which includes blades and hub, is variable, depending on the material that is used and on size of the blades. For a 2-3 MW turbine and 40 m blade length, the weight of the rotor is 40-50 tons. The hub rotor can reach very high weight because it is made entirely of steel, it is approximately 20 tons, almost a half of the entire weight of the rotor. All electric components are mounted into a structural element at the top of tower, which is called nacelle. It usually includes the low speed shaft, the high speed shaft, the gear box or drivetrain and the electric generator. A sketch of an upwind wind turbine can be seen in Figure 2.2.

The power associated to the flow, can be expressed with Eq. (2.1)

$$P_w = \frac{1}{2}\rho A U_w^2 \tag{2.1}$$

Where U_w is the mean wind speed vector, A is the cross section of the stream tube normal to average wind speed vector U_w and ρ is the density of air. If we consider a wind turbine with rotor area A_r, the extracted power can be defined by Eq. (2.2)

$$P_{aero} = \frac{1}{2}\rho A_r U_w^2 C_p \tag{2.2}$$

In particular it can be seen in Eq. (2.2) the introduction of a new factor C_p. It is a turbine power coefficient that depends on tip-speed ratio, $\lambda_{TSR} = \frac{\Omega R}{U_w}$ where Ω is the rotational speed of rotor, and on collective blades pitch β. The ability of a

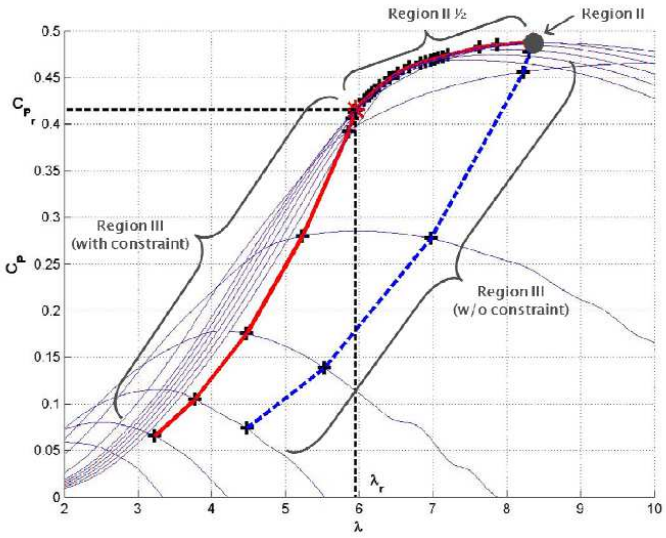

Figure 2.3: Chart of C_p trend, in function of λ and β. Sketch of different regions and its strategies

turbine to extract power from wind is defined by this factor, which has a theoretical limit defined by Betz limit, $C_p^{theor} \approx 0.59$. This represents an aerodynamic limit that can't be reached by any type of machine, in fact nowadays a typical turbine power coefficient is $C_p^{real} \approx 0.5$ at its maximum. However the real output of power is reduced by mechanical and electrical losses (η_m,η_{el}), then it can be defined as in Eq. (2.3).

$$P_{output} = \eta_m \eta_{el} P_{aero} \tag{2.3}$$

A typical control strategy is defined to keep an optimal efficiency for each wind value, in order to extract as much power as possible. A design parameter is the rated power value, P^R, that depends on the electrical grid, and on considerations about the wind Weibull curve. Instead the rated wind value, U_w^R, is defined by P^R and by Eq. (2.2), where C_p is completely defined by the structural model of the wind turbine, and depends on collective pitch, β and λ_{TSR}. Once defined U_w^R, the control strategy can be splitted into two regions:

- *Region II:* This region is defined by a U_w less than U_w^R. The consequence is that the P^R is not reached. The goal is to work with the C_p^{max} maximum, to extract a greatest possible power. In this region the controller tries to maintain λ_{TSR} as close as possible to λ_{TSR} of C_p^{max}, lowering Ω and maintaining a constant collective pitch as the wind speed grows. In terms of the speed, the region extends from U_{cut-in} to U_w^R.

- *Region III:* This region is defined by a U_w higher than U_w^R. Then P^R is always reached. The goal of the controller is to maintain this value of rated power, then

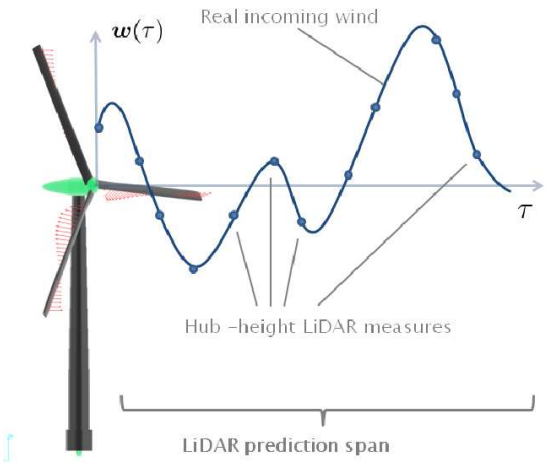

Figure 2.4: Example of LiDAR measuring hub-height windspeed

to do this it needs to work with the collective pitch and TSR, and maintaining a constant Ω, that is the rated rotor speed, Ω^R. The most effective control strategy makes use of actively controlled pitch actuators (there exist other more basic types of control, like stall-regulation control and the tilt-regulation control, which are not considered in this work). In terms of the speed, the region extends from U_w^R to $U_{cut-out}$.

.

This classification is the ideal case, but in most installations we must consider the *noise limit* as a project parameter. This implies that the Ω^R must be lower than the ideal case. Then between *Region II* and *Region III* a new region arises, called *Region* $II\frac{1}{2}$, where Ω^R is already reached but P^R is not. Since Ω is locked, the control strategy must compensate a variable TSR with an adjustment of pitch. This way, it is still possible to work with C_p values very close to the maximum. To better understand what we just explained it is useful to see Figure 2.3.

2.2 Control Techniques for Wind Turbines

This work explores three different control approaches. The first of these is the basic, non predictive LQR-integral, and it is used as reference. The others are two types of predictive control, that are to be tested. In particular the greatest difference between LQR-integral and predictive control, is that these last mentioned are feed-forward controllers. In fact wind information is used by these controllers to prepare the machine to an incoming wind event, e.g. a wind gust or a change in the average wind speed, Figure 2.4.

The improvement of the predictive controller with respect to the reference is that

the wind information not derived from an anemometer behind the rotor, but it's derived from a laser sensor placed on the hub. This technology, called LiDAR, scans the wind field in front of the turbine and provides a volumetric mean of the wind speed. Therefore the predictive control has access to an information on the wind before the same wind hit the turbine.

A quick description of the controllers is presented in the next sections. The intent is not to explain the implementation details of control method, but simply its main corresponding features. A more detailed description can be found in the reference [4], [32], [5], [6], [7].

2.2.1 LiDAR Techonology

The incoming wind information is a natural and perfect input for a predictive control law. Recent studies have led to a refinement of the technique able to detect the wind in front of the turbine. This technology is called LiDAR and usually placed on top of the tower, into the nacelle. The detection system uses a laser beam to hit some water or dust particles in the air in front of the turbine transported by the wind flow, and capturing their reflections, it is able to provide a detailed spatial description of the wind velocity field. Nowadays there are several experiments on real machines of different sizes, and the first results are encouraging in terms of the punctual reconstruction of the wind field. Clearly this is a recent technology, then in parallel to experiments in real environment, this sensor is also developing in different virtual simulators. For a comprehensive description of the topic see the references [4], [5], [10] and [9], in this section we discuss the main themes useful to understand this work and the next chapter.

In general a LiDAR simulator is developed to analyze a discrete wind field, Figure 2.5. The output of the LiDAR is a wind time series characterized by only one value of wind speed for time step. This value is obtained by a complex volumetric mean at each time instant. The volumetric mean is characterized by three spatial averages and one spatial interpolation. Clearly the laser beam does not intersect the exact point of the wind grid that represents the value of wind velocity in that spatial region. Therefore each point that it should be detected by laser beam, it is obtained by the first spatial interpolation between the four values of wind speed that surround it. The first mean is based on a series of data collected by the laser beam, this data are broken down by the number of focus that are considered, and for each focus there are several values as reference. This because the LiDAR can not detect the velocity of only one point, but to provide a exact value it must detect several values around it. After collecting at least 100 values for each focus a first mean is implemented, as explained after, with the Lorentz function. The laser beam follows an imposed pattern, which is split into multiple detection points. After the LiDAR detects each pattern sectors, the average is computed between these points. Therefore the output of the second average for each focus is provided. The last step of the volumetric mean is a simple average between the values of each focus at each time instant.

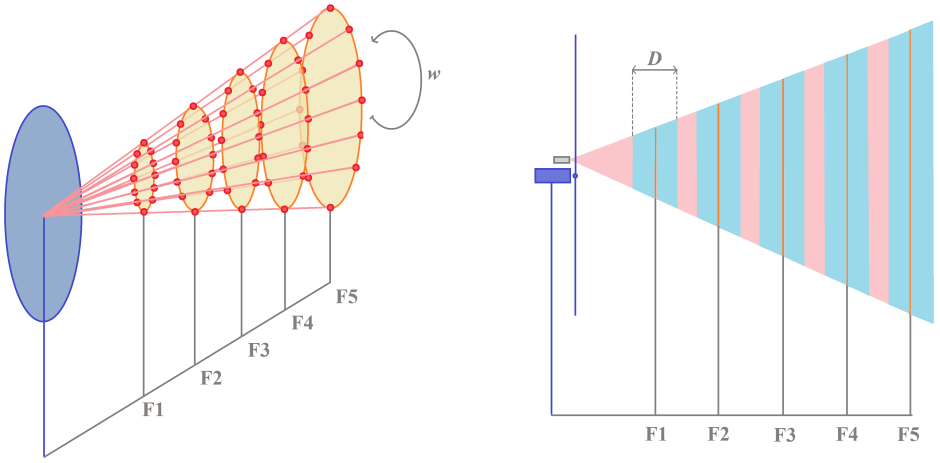

Figure 2.5: Sketch of the LiDAR sensor and the main characteristics of the detection system. In the first sketch it is represents the laser beam, each pattern focus and each detection point of LiDAR. In the second sketch it is shown the sampling range in light blue.

Table 2.1: Main characteristics of the focuses

Focus	Distance to WT	Pattern Diameter
1	0.5 D	1/3 D
2	0.75 D	1/2 D
3	1 D	2/3 D
4	1.25 D	5/6 D
5	1.5 D	1 D

The LiDAR simulator developed by DAST-Polimi has 5 Hz as sampling frequency, that means 0.2 sec per beam position. The pattern, that is used, is a circle with 12 stops, then with step of 30 degrees. Therefore the laser beam completes the circle in 2.4 sec. The number of focus that is considered is five, only constraint that is imposed is the size of the last circle. In fact the circle diameter of last focus is equal to the turbine diameter. The latter data requires the inclination of the laser beam with respect to the longitudinal axis, which is perpendicular to the rotor. Therefore every circle diameter for each focus is determined. The main characteristics of the focuses can be noticed in Table 2.1.

A simple representation of a basic LiDAR structure can be seen in Figure 2.5, where w indicates the rotation speed of the sensor with counterclockwise direction. As it is explained in reference [4], [5] and [9], the sensor doesn't detect the particles velocity only in the focal points, because this procedure can introduce a large error in the prediction of incoming wind. Then the sensor records 101 speed values in 60 meters of range (in Figure 2.5 this range is indicated as D) centered on each focal

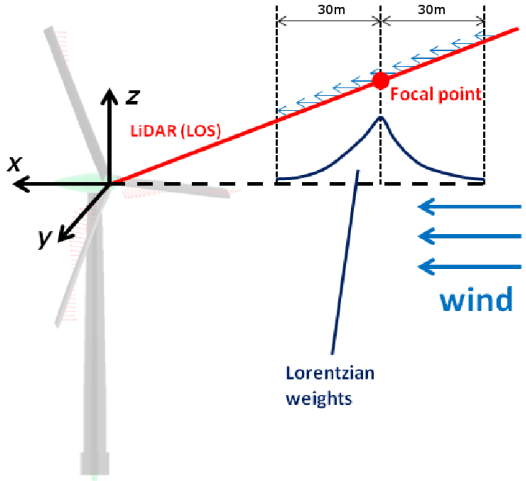

Figure 2.6: Simulation of LiDAR measurement at focal point: the measure is a weighted integral of the speed of 100 points within 60m centered on the focal point

point. After that, a weighted average is performed between these values, obtaining twelve speed values for each focal point. The weighing function can be based on the usual Lorentz profile (Figure 2.6), Eq. (2.4).

$$w(x, x_s) = \frac{e^{-4ln_2(\frac{x-x_s}{W})^2}}{\int_{\infty}^{\infty} e^{-4ln_2(\frac{x-x_s}{W})^2} dx} = \frac{2ln_2 e^{-4ln_2(\frac{x-x_s}{W})^2}}{W\sqrt{ln_2(\pi)}} \tag{2.4}$$

Where x_s is the designated focal distance ahead of the rotor, and the parameter W defines the span of the weighting function.

As described above after the LiDAR completes the first rotation, then after it has collected the first tranche of twelve values, it starts with the second average between these. An important characteristic of the LiDAR simulator developed by DAST-Polimi, is that this second average it is updated after each sampling instant of the LiDAR and not after each rotation of laser beam. The consequence of this peculiarity is that the LiDAR provides a value of wind speed for each sampling instant of the LiDAR, 0.2 sec, and not for each time rotation, 2.4 sec. Finally the last average is computed between the five values obtained from the second average, one for each focus.

In particular the wind value seen from the turbine is also a time series and it can be expressed by Eq. (2.5)

$$U_w(t) = \frac{1}{5}\sum_{n=1}^{5} U_n(t - t_{Preview_n}) \tag{2.5}$$

Where $t_{Preview_n}$ is a *'time-shifted'* according to Taylor's frozen turbulence hypothesis, and it is used to compute the correct average.

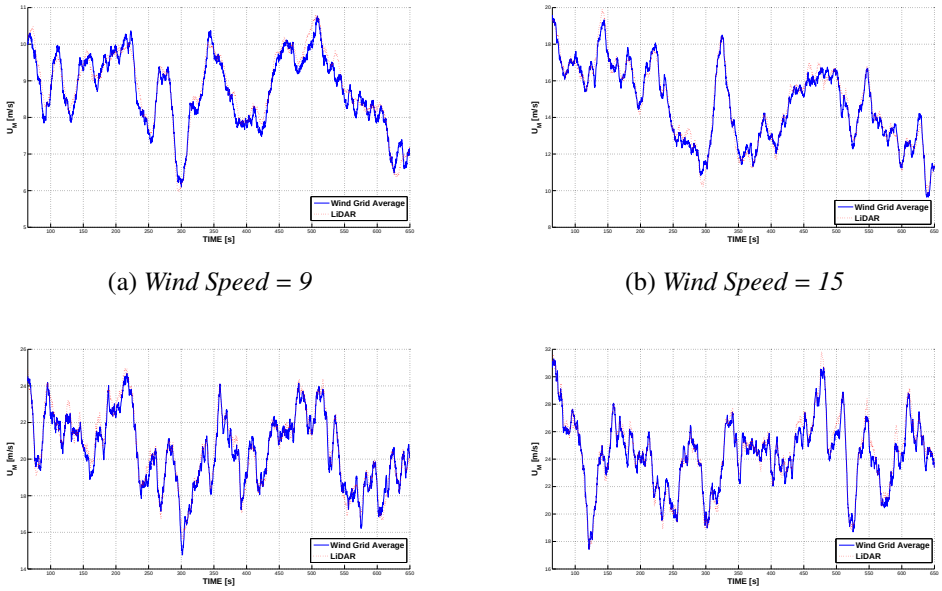

(a) *Wind Speed = 9* (b) *Wind Speed = 15*

(c) *Wind Speed = 21* (d) *Wind Speed = 25*

Figure 2.7: Comparison between Output LiDAR and wind grid average for each time instant

To verified the goodness of the output of the LiDAR simulator a comparison between it and simple average of discrete wind grid at each time instant is computed. The discrete wind grid as a function of time is obtained by using TurbSim code. The comparison is can be seen in Figure 2.7, for several speed simulation. It can be noticed that the difference between the these two signals is very low.

2.2.2 Linear Quadratic Regulator

The reduced model which is used for the synthesis of the LQR, can be seen in Figure 2.8. The considered set of states is composed by the fore-aft displacement of the tower head, d, and its time derivative $\dot{d}$; the rotor rotational speed Ω that it's measured on the low speed shaft; the measured pitch angle β_e and its time derivative $\dot{\beta}_e$; and the measured generator torque T_{el_e}. The red arrows are the components of the input array: collective pitch β_c and electric torque T_{el_c}. F_a and M_a are the aerodynamic loads considered in this reduced model, while T_l is the loss of torque due to effects of mechanical friction. Finally M_T, K_T and C_T are respectively mass, stiffness and damping of a second order system modeling the fore-aft dynamics of the tower head, based on a modal description of the tower dynamics truncated at the first mode.

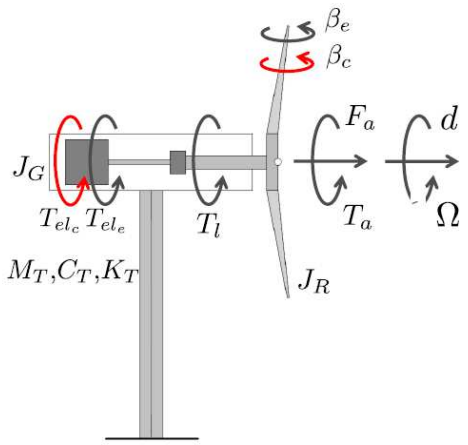

Figure 2.8: Scheme of the reduced model considered for the synthesis of the LQR control law

Therefore the following system of equations can be written for the reduced model:

$$(J_R + J_G)\dot{\Omega} + T_l(\Omega) + T_{el_e} - T_a(\Omega, \beta_e, U_w - \dot{d}, U_m) = 0 \tag{2.6a}$$

$$M_T\ddot{d} + C_T\dot{d} + K_T d - F_a(\Omega, \beta_e, U_w - \dot{d}, U_m) = 0 \tag{2.6b}$$

$$\ddot{\beta}_e + 2\zeta\omega\dot{\beta}_e + \omega^2(\beta_e - \beta_c) = 0 \tag{2.6c}$$

$$\ddot{T}_{el_e} + \frac{1}{\tau}(T_{el_e} - T_{el_c}) = 0 \tag{2.6d}$$

Where second order equation, Eq. (2.6a), are for the rotational dynamics of rotor. Equation 2.6b is the tower fore-aft dynamic equation. The last two are implemented to model the dynamics of actuators: a second order equation for pitch actuator and first order equation for the generator (torque actuator). In particular it can be noticed the presence of aerodynamic loads T_a and F_a in Eq. (2.6a) and (2.6b) that depend on several terms. The reason lies in the definition of aerodynamic torque and force exerted on the rotor:

$$T_a = \frac{1}{2}\rho\pi R^3 \frac{C_{P_e}(\lambda, \beta_e, U_m)}{\lambda}(U_w - \dot{d})^2 \tag{2.7a}$$

$$F_a = \frac{1}{2}\rho\pi R^2 \frac{C_{F_e}(\lambda, \beta_e, U_m)}{\lambda}(U_w - \dot{d})^2 \tag{2.7b}$$

Where C_{P_e} and C_{F_e} are non-dimensional torque and force factors, while R is the radius of rotor. Another term needs clarification: U_m is defined as the axial speed averaged over the rotor and over a suitably large time frame. Therefore the wind speed can be defined as $U_w = U_m + u_t$, u_t representing the turbulent fluctuations. The

aerodynamic thrust force and aerodynamic torque, as tip speed ratio λ, are related to the square of the actual wind speed seen by the rotor, which is the difference $(U_w - \dot{d})$.

The nonlinear reduced model, described by Eq. (2.6), can be easily linearized for a given equilibrium condition, defined by a given state and input set point corresponding to an assigned value of the wind speed U_m^*. In analytical terms, a trim condition is defined by a reference $\{\mathbf{x}^*, \mathbf{u}^*, U_m^*\}$, the turbulent fluctuation having been set to zero, $u_t = 0$. Therefore the nonlinear system can be rewritten in the form

$$\dot{\mathbf{x}} = \mathbf{f}(\mathbf{x}, \mathbf{u}, U_m) \tag{2.8}$$

where:

- *State array:* $\mathbf{x} = (d, \dot{d}, \Omega, \beta_e, \dot{\beta}_e, T_{el_e})^T$
- *Input array:* $\mathbf{u} = (\beta_c), T_{el_c}$

Then this can be linearized to give a form like

$$\Delta\dot{\mathbf{x}} = \mathbf{A}(\mathbf{x}, \mathbf{u}, U_m)\Delta\mathbf{x} + \mathbf{B}(\mathbf{x}, \mathbf{u}, U_m)\Delta\mathbf{u} \tag{2.9}$$

where:

- $\Delta\mathbf{x} = \mathbf{x} - \mathbf{x}^*$
- $\Delta\mathbf{u} = \mathbf{u} - \mathbf{u}^*$

Notice that in practice the linearization can be completed following a differentiation of the system 2.6. To identify the actual values of the coefficients of the **A** and **B** matrices it is possible the use of a simulator like $Cp - Lambda$. In fact to know these matrix coefficients it is necessary to know the derivatives $\frac{\partial C_{T_e}}{\partial \mathbf{x}}, \frac{\partial C_{T_e}}{\partial \mathbf{u}}$, where the torque coefficient C_{T_e} is by definition $C_{T_e} = \frac{C_{P_e}}{\lambda}$, and similar derivatives for C_{F_e}. These coefficients are computed as punctual functions of λ and β_e from $Cp - Lambda$, therefore these derivatives can be calculated numerically.

The linearization is performed for a given value of U_m. This represents a parameter of the linearization, which must cover the entire length of the wind field (from U_{cut-in} to $U_{cut-out}$).

After this the linearized system can be rewritten as

$$\Delta\dot{\mathbf{x}} = \mathbf{A}(U_m)\Delta\mathbf{x} + \mathbf{B}(U_m)\Delta\mathbf{u} \tag{2.10}$$

The theory behind the LQR design is based on the cost function minimization over an infinite time horizon, imposing the dynamics of the linearized system as a constraint.

$$J = \frac{1}{2}\int_0^\infty (\Delta\mathbf{x}^T\mathbf{Q}\Delta\mathbf{x} + (\Delta\mathbf{u}^T\mathbf{R}\Delta\mathbf{u}))dt \tag{2.11}$$

With this cost function and this shape of the linearized system, the optimal control solution can be obtained in closed form for a given U_m as

$$\Delta\mathbf{u} = -\mathbf{R}^{-1}\mathbf{B}^T\mathbf{P}\Delta\mathbf{x} \tag{2.12a}$$

$$\mathbf{PA} + \mathbf{A}^T\mathbf{P} - \mathbf{P}\overline{\mathbf{R}}\mathbf{P} + \mathbf{Q} = 0 \tag{2.12b}$$

$$\overline{\mathbf{R}} = \mathbf{B}\mathbf{R}^{-1}\mathbf{B}^T \tag{2.12c}$$

where $\mathbf{P}$ is matrix that solves the algebraic Riccati equation, Eq. (2.12b). While, in Eq. (2.12a), $\mathbf{R^{-1}B^TP}$ can be considered as a unique gain matrix, which is called $\mathbf{K}$. Since the value of U_m is equal to the value provided from the anemometer placed on the nacelle (U_w), filtered by the turbulent component (u_t), it is possible to find the control input as

$$\mathbf{u} = -\mathbf{K}(U_m)(\mathbf{x} - \mathbf{x}^*(U_m)) + \mathbf{u}^*(U_m) \tag{2.13}$$

The reduced model *cit*, although rather complete and complex, is an approximation of the reality. It is useful in some cases to use an augmented model, represented by control *LQR-integral*, find more details in [4]. The new state includes in addition to the old parameters also one integral, as defined $\int \Omega dt$. Therefore the new augmented state is $\mathbf{x}_{aug} = (d, \dot{d}, \Omega, \beta_e, \dot{\beta}_e, T_{el_e}, \int \Omega dt)$; while the new linearized state equation can be written as

$$\Delta\dot{\mathbf{x}}_{aug} = \mathbf{A}_{aug}(\mathbf{x}^*, \mathbf{u}^*, U_m^*)\Delta\mathbf{x}_{aug} + \mathbf{B}_{aug}(\mathbf{x}^*, \mathbf{u}^*, U_m^*)\Delta\mathbf{u}_{aug} \tag{2.14}$$

where:

$$\mathbf{A}_{aug}(\mathbf{x}^*, \mathbf{u}^*, U_m^*) = \begin{bmatrix} & & & & & & \\ & \mathbf{A}(\mathbf{x}^*, \mathbf{u}^*, U_m^*) & & & & & \\ & & & & & & \\ \begin{bmatrix} 0 & 0 & 1 & 0 & 0 & 0 \end{bmatrix} & & & & & & 0 \end{bmatrix} \tag{2.15}$$

and

$$\mathbf{B}_{aug}(\mathbf{x}^*, \mathbf{u}^*, U_m^*) = \begin{bmatrix} \mathbf{B}(\mathbf{x}^*, \mathbf{u}^*, U_m^*) \\ \begin{bmatrix} 0 & 0 \end{bmatrix} \end{bmatrix} \tag{2.16}$$

The LQR accounting for a integral state allows a better control performance on the rotational speed, both in deterministic and especially turbulent conditions.

2.2.3 Predictive Controllers

The type of control described above has a small defect: the wind information, that is used by controller, is provided by an anemometer placed *behind* the rotor. Therefore the value of U_w, that is detected by the measuring device, is referred to a wind history that has already passed through the rotor. Also we must consider other two issues, the amount of time to read the information, and the control action to react to it.

Therefore the LQR control is from the start less performing, as it has no access to any predictive information. One way to solve this problem is to design a control that can use wind information measured at a certain distance from the turbine. The technology that allows to predict the incoming wind is the LiDAR sensor (Light Detection And Ranging). The predictive taken into account for this work are Non-Homogeneous LQR (NHLQR) and Receding Horizon Control (RHC).

Receding Horizon Control

The basic idea behind the RHC control is that of solving a cost function optimization problem on a finite time window instead of considering an infinite window. The new cost function may be defined as

$$J = \frac{1}{2}\left(\Delta\mathbf{x}^T(T_f)\mathbf{Q}_f\Delta\mathbf{x}(T_f) + \int_0^{T_f}(\Delta\mathbf{x}^T\mathbf{Q}\Delta\mathbf{x} + \Delta\overline{\mathbf{u}}^T\mathbf{R}\Delta\overline{\mathbf{u}})dt\right) \tag{2.17}$$

and its minimization is subjected to the dynamics system that may be defined as

$$\Delta\dot{\mathbf{x}} = \mathbf{A}(\mathbf{x}^*, \mathbf{u}^*, U_m^*)\Delta\mathbf{x} + \mathbf{B}(\mathbf{x}^*, \mathbf{u}^*, U_m^*)\Delta\mathbf{u} + \mathbf{G}(\mathbf{x}^*, \mathbf{u}^*, U_m^*)\Delta\omega \tag{2.18}$$

where $\mathbf{x}^*$ and $\mathbf{u}^*$ are respectively the states and controls array at the trim point of wind speed U_m^*. Meantime $\Delta\omega = \omega - \omega^* = U_w - U_m^*$ is defined as an exogenous input. An advantage of this formulation is the possibility to naturally put inequality constrains in the optimization problem, in the form $\mathbf{D}\Delta\mathbf{x} + \mathbf{E}\Delta\mathbf{u} \leqslant 0$, which may be helpful to account for control time-rate limitations, e.g pitch rate, directly in the optimization problem. The obvious disadvantage is that there is no closed form solution to the optimization problem. In order to apply existing numerical solving schemes it necessary to switch to a discretized formulation, based on both a discretized cost function and state equation.

Consider a discretization of the prediction window T_f by N steps.

- *The Cost Function*

$$\widehat{J} = \frac{1}{2}\left(\Delta\mathbf{x}_N^T\mathbf{Q}_f\Delta\mathbf{x}_N + \sum_{k=1}^{N}(\Delta\mathbf{x}_k^T\mathbf{Q}\Delta\mathbf{x}_k + \Delta\mathbf{u}_k^T\mathbf{R}\Delta\mathbf{u}_k)\right) \tag{2.19}$$

- *Dynamics System*

$$\Delta x_{k+1} = \mathbf{A}_k\Delta x_k + \mathbf{B}_k\Delta u_k \tag{2.20}$$

- *Linear Inequality Constraints*

$$\mathbf{D}\Delta x_k + \mathbf{E}\Delta u_k \leqslant 0 \tag{2.21}$$

The solution of the optimization problem provides the control scheduling for each step within the prediction window. But only the first value is actually used and commanded to the actuators, after verifying the limits of the same.

Non Homogeneous LQR

This type of control is a natural extension of the basic LQR. In fact NHLQR is a controller that tries to overcome the limits of LQR, previously described. The dynamic system is the same of RHC, Eq. (2.18), and a typical cost function with infinite horizon ($T_f \rightarrow \infty$) already described in Eq. (2.11) is considered. The *'predictive'* component in the dynamic system introduces a *non homogeneous* term in the solution of the optimization problem. In fact the optimal control input has the following form

$$\Delta\overline{\mathbf{u}}(t) = -\mathbf{R}^{-1}\mathbf{B}^T\mathbf{P}\Delta\mathbf{x}(t) - \mathbf{R}^{-1}\mathbf{B}^T\int_t^\infty (e^{-\overline{\mathbf{A}}^T(t-\tau)}\mathbf{P}\mathbf{G}\Delta\omega(\tau))d\tau \tag{2.22}$$

where it can be noticed that the first term is equal to an optimal control input of basic LQR. Therefore Eq. (2.22) can be rewritten in the following compact form

$$\Delta\overline{\mathbf{u}}(t) = \Delta\mathbf{u}_{LQR}(t) + \Delta\mathbf{u}_{nh}(t) \tag{2.23}$$

where

$$\Delta\mathbf{u}_{nh}(t) = -\mathbf{R}^{-1}\mathbf{B}^T\int_t^\infty (e^{-\overline{\mathbf{A}}^T(t-\tau)}\mathbf{P}\mathbf{G}\Delta\omega(\tau))d\tau \tag{2.24}$$

In particular matrix $\overline{\mathbf{A}}$ is derived from the minimization of the cost functional and is equal to $\mathbf{A} - \mathbf{B}\mathbf{R}^{-1}\mathbf{B}^T\mathbf{P}$, and $\mathbf{P}$ solves the usual algebraic Riccati equation. This controller is important because it allows to include a predictive information without affecting the system stability. It is also possible to solve analytically the integral in Eq. (2.24), and then scheduling the gains of the control. But to do this, the only constraint is to consider the difference between incoming wind information provided by the LiDAR and reference wind value ($\Delta\omega$), as a piecewise constant. The reference value is evaluated as slowly varying moving average of the LiDAR information itself. Clearly this is a strong approximation, from the theoretical point of view, given that the output of the LiDAR is definitely not constant and it is only able to provide a prediction over a finite time span. Then Eq. (2.24) can be rewritten in following form:

$$\Delta\mathbf{u}_{nh}(t) = -\mathbf{R}^{-1}\mathbf{B}^T\overline{\mathbf{A}}^{-T}\mathbf{P}\mathbf{G}(\omega - \omega^*) \tag{2.25}$$

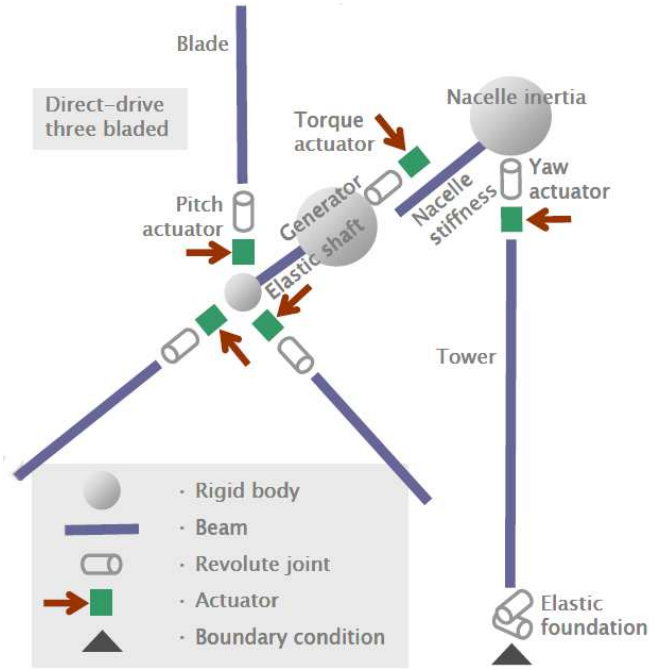

Figure 2.9: Sketch of the main Cp-Lambda elements

2.3 Simulators considered for this work

It is important to emphasize that all virtual simulations performed in this work have been done with the use of a simulator capable of describing the wind turbine dynamics. This simulator is *Cp-Lambda* (Code for Performance, Loads and Aeroelasticity by Multi-Body Dynamic Analysis), a code developed internally by DAST-Polimi. This software is a multi-body code, allowing a sophisticated description of the topology of a real horizontal-axis wind turbine, all the relevant rigid dynamics and those of the actuators, a detailed finite-element based modeling of many kind of beams and deformable structures, Figure 2.9.

Therefore the code has some peculiarities that allows to generate very realistic simulations:

- Geometrically exact composite beam models
- Generic topology (Cartesian coordinates and Lagrange multipliers)
- Dynamic wake model
- Efficient large-scale DAE solver
- Non-linearly stable time integrator
- Fully IEC 61400 compliant (DLCs, wind models)

But an important feature is the very nature of the model, which takes into account various effects, being an aero-servo-elastic model. So with a coupling between two models, a structural one and an aerodynamic one, it is possible to obtain realistic simulations.

Another simulator taken into account in this thesis is *TurbSim*, a code developed by National Renewable Energy Laboratory (NREL). It is a stochastic, full-field, turbulent-wind simulator. This allows to generate three wind files, one per component, which characterize a three-dimensional wind field. In particular, it allows to set, besides the main characteristics of the turbine, also the type of wind that you want to generate, namely the average of the simulation, the type of turbulence, and the boundary layer of the Earth.

Chapter 3

Unfrozen Incoming Wind for LiDAR Sensor

Nowadays most of LiDAR simulators are based on Taylor Hypothesis. This hypothesis is a strong approximation. It arise for comparison of some typical quantities of turbulence between experimental campaigns and Direct Numerical Simulation (DNS). These quantities, such as velocity-spectrum tensor and the energy-spectrum function, can be extracted from the DNS of turbulence but they cannot be detected directly from any experimental campaign because require the measurement of the two-point velocity correlation, which clearly is not feasible. However, thanks Taylor Hypothesis and with a single probe (e.g. a hot-wire anemometer) it is possible to approximate the measurement of two-point velocity correlation. Whereby this approximation allows to switch from time domain to space domain with only the average velocity information. In terms of LiDAR sensor this approximation enables to calculate the travel time of a wind field previously detected by the LiDAR at a defined distance. In fact, a value of average velocity must be provided to the LiDAR sensor. The time taken by air particles to reach the turbine is computed, by dividing the focal distance by the average speed. In this way the LiDAR sensor simulator is developed without taking into account the possibility that the velocity and turbulence can change over the distance from the detecting point to the turbine. The consequence is that the wind front that hits the turbine is not exactly the same measured by LiDAR. This implies that the predictive control prepares the machine with a wind information which is neither totally wrong nor perfect. In the last few years the need to go beyond this problem has emerged. The scope of the current research is to understand if the unfrozen theory can introduce a real improvement in the prediction of the incoming wind, and how many differences there are between a frozen and unfrozen model.

In this chapter in the first section there is an extensive description of unfrozen model, derived from the Kirstensen theory, reference [13]. Therefore the mathematical model is described. After this a test model that generating a simple wind time series (one-point grid) to verified the goodness of the unfrozen model is explained. As parameter of goodness, the coherence between different signals is taken into account.

Once verified that the unfrozen model allows to generating a reasonable unfrozen wind time series, a more complete and more complex description of generator of wind filed is reported. Therefore it is described how all these tools can change the available frozen LiDAR to a new unfrozen LiDAR, that it is used in this work. The last section describes the implementation aspects that we faced in this work, in particular the risk of a large amount of data storage and the possibility that the time of simulation explode.

3.1 Unfrozen Turbulence

The unfreezing of turbulence is based on a theory arisen in the Seventies of the last century. The greatest protagonist of the development of an unfrozen model was Kirstensen with his main article, reference [13]. His theory is based on different articles written in the same period, references [22], [20], [19], [21]. The basic idea behind the unfrozen turbulence is the determination of a longitudinal spectral coherence function, that it is rather different from transversal coherence function. In the paper by Pielke and Panofsky, reference [20] it is suggested that the coherence has the form

$$coh(n) = e^{-a\frac{nD}{U_0}} \tag{3.1}$$

where n is the frequency in Hz, U_0 is the time averaged velocity and D is the displacement between two position in space. In particular the parameter a is a dimensionless *decay factor* of order 10. Clearly if we consider the Taylor Hypothesis the longitudinal coherence is unit. The idea that the coherence has the form written in Eq. (3.1) is verified by Davenport, reference [16], with an analysis of data from vertically displaced cup anemometers in a experimental campaign. After Pielke and Panofsky several developments appeared, but essentially the main equation of longitudinal coherence is unchanged.

3.1.1 Kirstensen Model

Kirstensen model is based on a longitudinal coherence between two points at the distance D from each other. The model represents the possibility that an eddy, with particular characteristics in terms of mean velocity and size, which is detected by the first anemometer, can reach the second anemometer with the same characteristics or with some variations. A sketch of this type of experiment can be noticed in Figure 3.1.

Where U_0 is the time averaged velocity of the incoming wind, and λ is the size of the vortex. With this data it's possible to determine the eddy frequency $n \approx \frac{U_0}{\lambda}$. Another important term for this model, representing the decay of the vortex, is the *eddy turnover time*, τ_λ. The contributions which impose a decay to the vortex can be purely longitudinal or with a combination between a longitudinal decay and a lateral drift. Then it should be possible to develop two different models: *Longitudinal Model* and *Longitudinal Transversal Model*.

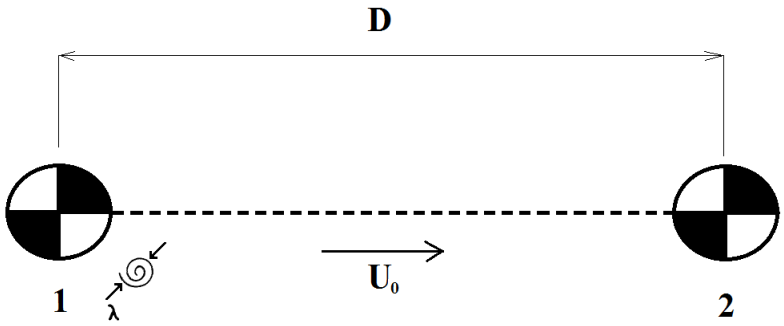

Figure 3.1: A experimental model that is considered by Kirstensen to develop his numerical model

Longitudinal Model

This model is based on a purely longitudinal decay, that is defined by turbulent kinetic energy per unit wavelength, $B(\lambda)$. In fact the eddy turnover time is described by Eq. (3.2).

$$\tau_\lambda \approx \left(\frac{B(\lambda)}{\lambda}\right)^{-1/2} \tag{3.2}$$

where $B(\lambda)$ is defined by [14] as:

$$B(\lambda) = \frac{2\pi}{\lambda^2} E\left(\frac{2\pi}{\lambda}\right). \tag{3.3}$$

In particular the turbulent kinetic energy per unit wavelength is approximately defined as a function of frequency range. In fact there are mainly two different frequency ranges: *Inertial Sub-range*, *Energetic Range*.

In inertial sub-range, [12], which means $\lambda < l$ where l is the scale of turbulence, $B(\lambda)$ is entirely defined by λ and ε. Then $B(\lambda)$ has the following form

$$B(\lambda) \approx \varepsilon^{2/3} \lambda^{-1/3} \tag{3.4}$$

where ε is the rate of dissipation of turbulent kinetic energy and is defined as

$$\varepsilon \approx \frac{\sigma^3}{l} \tag{3.5}$$

Then it is possible to rewrite the eddy turnover time for the inertial sub-range case:

$$\tau_\lambda \approx \frac{l^{1/3} \lambda^{2/3}}{\sigma}. \tag{3.6}$$

Viceversa in the general case, when the inertial condition is not satisfied, it is possible to introduce a new parameter, that it's called g. It is a dimensionless function of the parameter $\frac{l}{\lambda}$. This parameter is defined by experimental campaign and has the role of adjusting the definition of turbulent kinetic energy defined in inertial sub-range (Eq. 3.4). Then the new form of $B(\lambda)$ is the following equation

$$B(\lambda) \approx \varepsilon^{2/3}\lambda^{-1/3} g\Big(\frac{l}{\lambda}\Big) \tag{3.7}$$

and the eddy turnover time is

$$\tau_\lambda \approx \Big(\frac{l^{1/3}\lambda^{2/3}}{\sigma}\Big) g^{-1/2}\Big(\frac{l}{\lambda}\Big). \tag{3.8}$$

Once determined the eddy turnover time, we need to define the probability that the eddy detected by the first anemometer can *hit* the second target. Since the time t of travel from station 1 to station 2 is D/U_0 the probability P_1 that an eddy does not decay during the transport is hypothesized to be

$$P_1 \approx e^{-\frac{D}{U\tau_\lambda}} \tag{3.9}$$

then the coherence for a purely longitudinal model is

$$coh(n) = P_1^2. \tag{3.10}$$

Longitudinal Transversal Model

On the contrary this model is more complex. It's developed on the combination of two contributions. As the name indicates, it is constituted by a longitudinal effect of decay and a transversal one. Then the coherence is defined by the following equation:

$$coh(n) \approx P_1^2 P_2^2 \tag{3.11}$$

Where P_1 is just defined in Eq. (3.9). Instead P_2 indicates the probability that a vortex detected by the first station is still detected in the second station, taking into account the possibility of dissipation due to the amount of transversal turbulent diffusion during the travel between the two stations. The definition of P_2 is more complex than P_1 and also for this parameter several experimental campaigns were carried out in the past. For a complete mathematical proof see reference [13], here the main steps are illustrated.

Before explaining the mathematical model it is helpful to itemize the three assumptions which characterize the model:

- *First Assumption:* The transversal Lagrangian velocity, v_t is stationary. Then

$$\sigma_t^2 = \int_0^{D/U} dt' \int_0^{D/U} dt'' < v_t(t')v_t(t'') > \tag{3.12a}$$

$$\approx 2\sigma^2 \frac{D}{U} \int_0^{D/U} \left(1 - \frac{U_\tau}{D}\right)\rho_L(\tau)d\tau \tag{3.12b}$$

  where the brackets denote ensemble averaging and the function $\rho_L(\tau)$ is the Lagrangian autocorrelation function.

- *Second Assumption:* In order to reduce the number of parameters the variance of v_t is equal to σ^2. Consequently it can be approximated σ_t^2 with the following

$$\sigma_t^2 \approx \begin{cases} \left(\frac{\sigma}{U}\right)^2 D^2 & \text{if } \frac{\sigma}{U}\frac{D}{l} \leqslant 1 \\ \frac{\sigma}{U} Dl & \text{if } \frac{\sigma}{U}\frac{D}{l} \geqslant 1 \end{cases} \tag{3.13}$$

- *Third Assumption:* the transversal diffusion is considered as an axisymmetric Gaussian transversal diffusion

Then the probability P_2 has the following form:

$$P_2 = \int_0^{\lambda} rdr \int_0^{2\pi} d\phi \frac{e^{-\frac{r^2}{2\sigma_t^2}}}{2\pi\sigma_t^2} = 1 - e^{-\frac{\lambda^2}{2\sigma_t^2}}. \tag{3.14}$$

With this definition of P_2 we can rewrite Eq. (3.11):

$$coh(n) = e^{-2\alpha G \frac{nl}{U_0}} \begin{cases} (1 - e^{-(2\alpha^2\left(\frac{nl}{U}\right)^2)^{-1}})^2 & \text{for } \alpha \leqslant 1 \\ (1 - e^{-(2\alpha\left(\frac{nl}{U}\right)^2)^{-1}})^2 & \text{for } \alpha \geqslant 1 \end{cases} \tag{3.15}$$

where

$$\alpha = \frac{\sigma}{U}\frac{D}{l} \tag{3.16}$$

and

$$G(\zeta) = 33^{-2/3} \frac{(33\zeta)^2(33\zeta + \frac{3}{11})^{1/2}}{(33\zeta + 1)^{11/6}} \tag{3.17}$$

It's useful to emphasize what is the origin of Eq. (3.17). Assuming isotropy and neutral lapse rates, as it is written in reference [13] and [17], $G(\zeta)$ is a semi-empirical expression, in the Kaimal spectrum case, where $\zeta = \frac{l}{\lambda} = \frac{nl}{U}$.

3.1.2 Test Model

Once developed the unfrozen turbulence model, the next step is create a wind model to verify the goodness of unfreezing. Therefore a simple wind time series is chosen, which is composed of a constant in time value, that represents the wind mean velocity, and a fluctuation part, that represents the turbulent contribute.

$$U_k(t) = U_{k_0} + u_k(t) \qquad \text{where } k = u, v, w \tag{3.18}$$

Where U_{k_0} is the wind mean velocity, and $u_k(t)$ is the turbulence fluctuation. In particular $u_k(t)$ can be written in the following form

$$u_k(t) = \sum_{i=1}^{N} S_k(n_i) cos(2\pi n_i t + \phi_{k_i}). \tag{3.19}$$

The turbulent fluctuation is determined by the magnitude of the turbulent spectrum, $S_k(n_i)$, where n_i is the frequency value. Another important parameter in Eq. (3.19) is the value of ϕ_{k_i}, that represents a random seed, one for each frequency, which introduces randomness in the generation of turbulence. In particular the frequency range is determined as a function of the time window and the time steps, accordingly with Nyquist sampling theorem. Instead for the form of turbulence spectrum we refer to the reference [18]:

$$S_k(n_i) = \frac{4\sigma_k^2 \frac{L_k}{U_{k_0}}}{(1 + 6n_i \frac{L_k}{U_{k_0}})^{5/3}} \tag{3.20}$$

It can be noticed that Eq. (3.20) represents the *Kaimal Turbulent Spectrum*, where L_k is the integral scale parameter, that it is defined as

$$L_k = \begin{cases} 8.10\Lambda_U & \text{for } k = u \\ 2.70\Lambda_U & \text{for } k = v \\ 0.66\Lambda_U & \text{for } k = w \end{cases} \tag{3.21}$$

with

$$\Lambda_U = \begin{cases} \begin{cases} 21 & \text{HH} < 30 \\ 0.7 \cdot HH & \text{HH} > 30 \end{cases} & \text{Edition} \rightarrow 2 \\ \begin{cases} 42 & \text{HH} < 60 \\ 0.7 \cdot HH & \text{HH} > 60 \end{cases} & \text{Edition} \rightarrow 3 \end{cases} \tag{3.22}$$

where HH is the height of the hub. For this work the *Edition 3*, which refers to a scale parameter [33] [25], is considered. In addition there is a further term to be determined, σ_k. The value of standard deviation is defined as follows

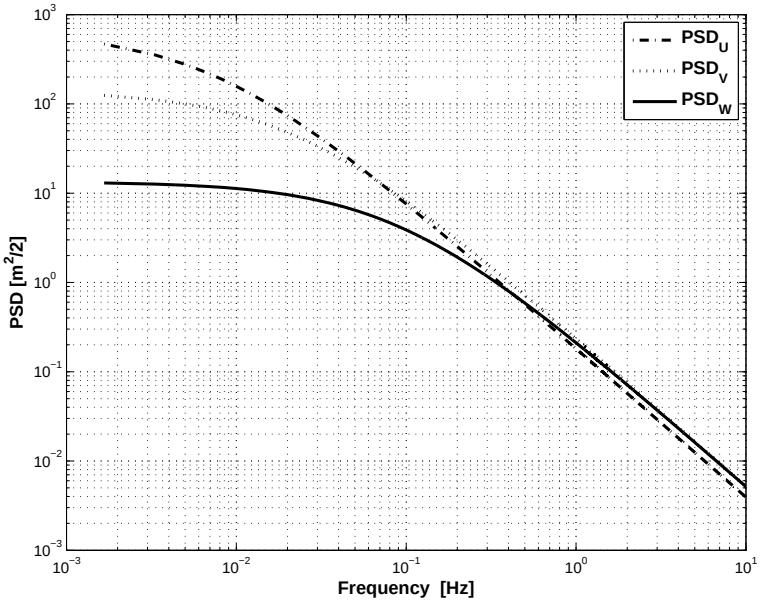

Figure 3.2: Turbulent Spectrum with mean velocity equal to 15 m/s, and 600 sec of time window

$$\sigma_k = \begin{cases} \sigma_{IEC} & \text{for } k = u \\ 0.8\sigma_{IEC} & \text{for } k = v \\ 0.5\sigma_{IEC} & \text{for } k = w \end{cases} \tag{3.23}$$

where

$$\sigma_{IEC} = TurbInt(0.75U_{k_0} + 5.6) \tag{3.24}$$

As required by International Standard, a value of turbulent intensity, $TurbInt$, has been chosen equal to 16%, which corresponds to a turbulence of type A, namely that of maximum intensity. After this it should be possible to reconstruct the turbulent spectrum as a function of frequency. The trends are shown in Figure 3.2

In the first analysis a wind field with only one grid point has been generated. The longitudinal mean velocity, U_{u_0}, is equal to 15 m/s, and with $U_{v_0} = U_{w_0} = 0$. A simulation time of 600 *sec* is considered, with time steps equal to 0.05 *sec*. The result has the shape shown in Figure 3.3

Therefore to recreate an unfrozen wind time history it is necessary to set up two different time histories, one for the start of the simulation and one to set the evolution parameter of unfrozen wind. In fact the unfrozen wind represents the evolution of the seed of the first wind towards the seed of the second one. To do this it is important to define the unfreezing model, for this purpose the most complete is chosen, i.e. *Longitudinal Transversal Model*. The evolution is represented by the following equation

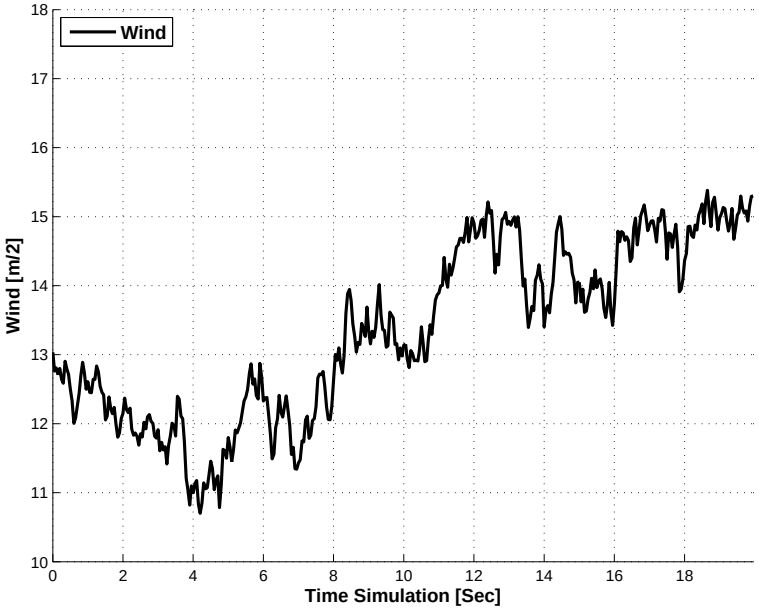

Figure 3.3: Example of wind time history for the component u

$$\Phi_{i_{unfrozen}} = f_i \phi_{i_{frozen,1}} + (1 - f_i)\phi_{i_{frozen,2}} \tag{3.25}$$

where f is defined as

$$f_i = \sqrt{coh} = P_1 P_2. \tag{3.26}$$

In particular it can be noticed that P_1 and P_2 depend on the wind components (u, v, w),then we have three different trends of f, one for each component. They can be seen in Figure 3.4

Then the unfrozen wind field can be written, always as a sum of two contributions: mean wind speed, and turbulent fluctuation.

$$U_{k_{unfrozen}}(t) = U_{k_0} + \sum_{i=1}^{N} S_k(n_i) cos(2\pi n_i t + \Phi_{i_{unfrozen}}) \tag{3.27}$$

It is important to emphasize what are the key parameters that influence the unfrozen wind field. As written above the fundamental parameter is the seed of the wind, because it can be considered as the fingerprint of the wind. The α parameter is hidden in f, Eq. (3.16). It is another fundamental quantity because changing it will change the unfrozen wind trend. This parameter determines how rapidly the coherence decreases with the dimensionless frequency $\frac{nl}{U_0}$, reference [13], and it's closed related to of the decay of turbulence. In fact, in Eq. (3.15) it was assumed that the decay part is an exponential function of time of travel, t, divided by an eddy lifetime, τ_λ

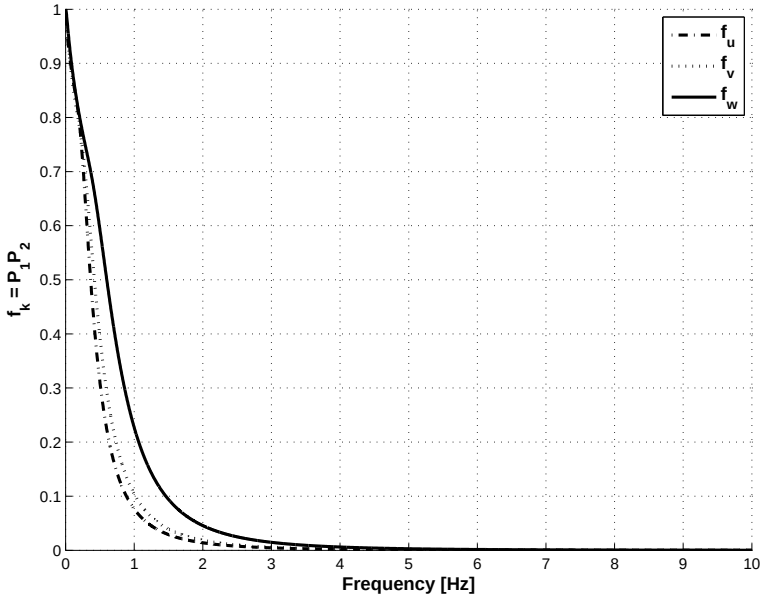

Figure 3.4: Trends of longitudinal coherence, f, as a function of frequency for each wind component

$$a = \frac{t}{\tau_\lambda} \approx \frac{\sigma}{U_0}\frac{D}{l}\frac{nl}{U_0} \tag{3.28}$$

where it can be noticed the presence of α parameter. The value of this quantity depends on two variables, D and U. While U is the mean velocity of each considered simulation, D represents the distance between two anemometers, then the distance between the reference point and the point that we want to unfreeze. In particular the magnitude of this distance can not be considered in absolute terms, but in relation with the integral scale, L_k, and its magnitude.

As it can be seen in Figure 3.5 the trend of unfrozen wind is quite similar to Frozen 1. The reason for this behavior is because the value of D, that it is considered, is equal to 150 meters, while the value of averaged time speed of wind is equal to 15 m/s. If we take a hub height equal to 80 meters and the intensity of turbulence equal to 16%, we obtain the integral scale l equal to 56 m and σ equal to 2.69 m/s. After this consideration of data simulation the decay parameter can defined as a function of frequency n : $t/\tau_\lambda \approx 1.8n$. It's clear how at low frequencies the value of the turbulent decay is rather low. In fact, if $t/\tau_\lambda \approx 0$ we obtain a value of coherence equal to 1, then the Frozen Hypothesis.

This reasoning can be verified by looking at the charts of coherence, Figure 3.6. In fact, as expected there is a higher coherence between Frozen 1 and Unfrozen at low frequencies. This means that the signal represented by Unfrozen is quite similar to Frozen 1, because the low frequencies are those with grater energy. Therefore the two trends are close. Viceversa at the high frequencies there is a greater coherence between

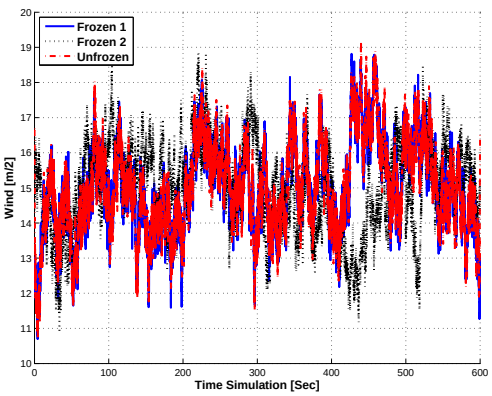

(a) *Wind Field, component u*

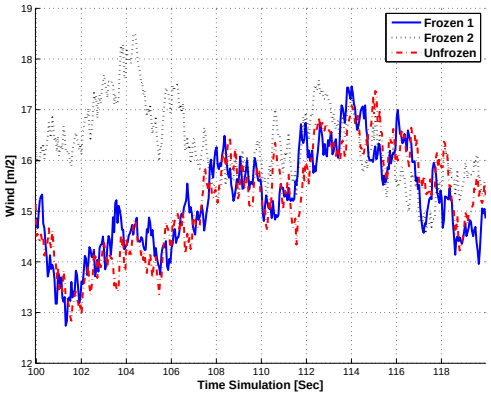

(b) *Wind Field, component u, focus 20 sec*

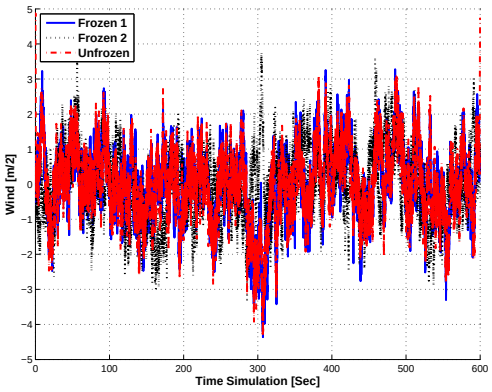

(c) *Wind Field, component v*

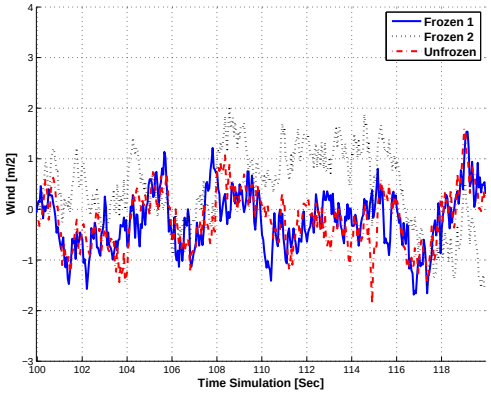

(d) *Wind Field, component v, focus 20 sec*

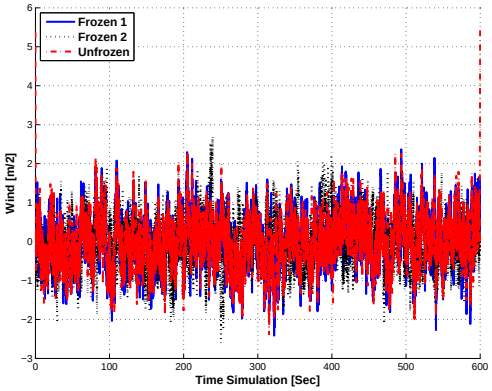

(e) *Wind Field, component w*

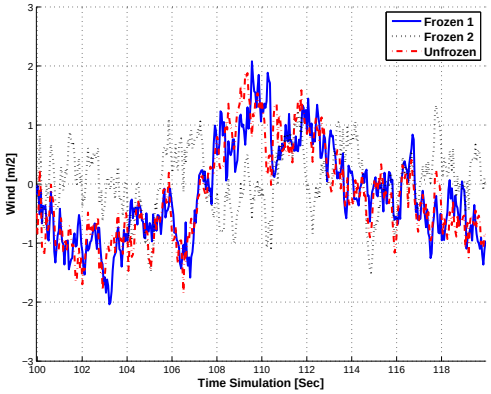

(f) *Wind Field, component w, focus 20 sec*

Figure 3.5: Comparison between trends of wind time histories: Frozen 1, Frozen 2 and Unfrozen

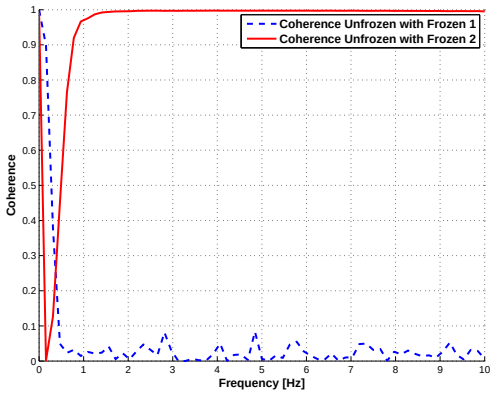

(a) *Coherence Trend for component u*

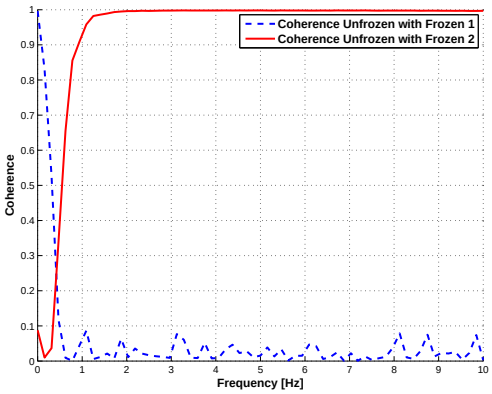

(b) *Coherence Trend for component v*

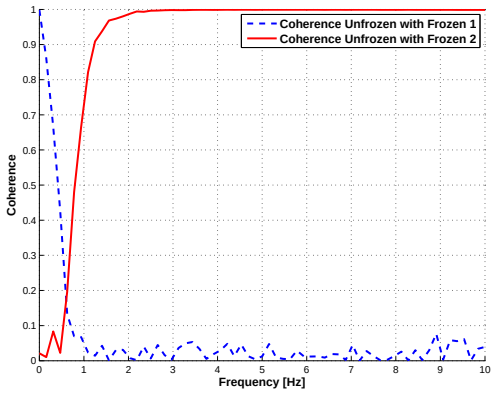

(c) *Coherence Trend for component w*

Figure 3.6: Comparison between trends of Frozen 1, Frozen 2 and Unfrozen longitudinal coherence

Frozen 2 and Unfrozen. The consequence is that the high perturbations of wind field are close between these two seeds of wind.

To underline the importance of the decay parameter, it is useful to see the Figures 3.7 and 3.8. Where in the first it can be noticed the difference between three coherence analysis of three different unfrozen wind histories, changing the distance from the turbine. In the second one it can be seen how three different values of averaged time wind speed can influence the decay of turbulence. Three different coherence analysis are done, changing only mean velocity.

3.2 Unfrozen Wind Field

The test model to generate a casual wind history is a simple code that takes into account only one grid point and a sinusoidal signal with a random phase. To generate a complex wind field with a finer grid, it is necessary to develop a new wind model.

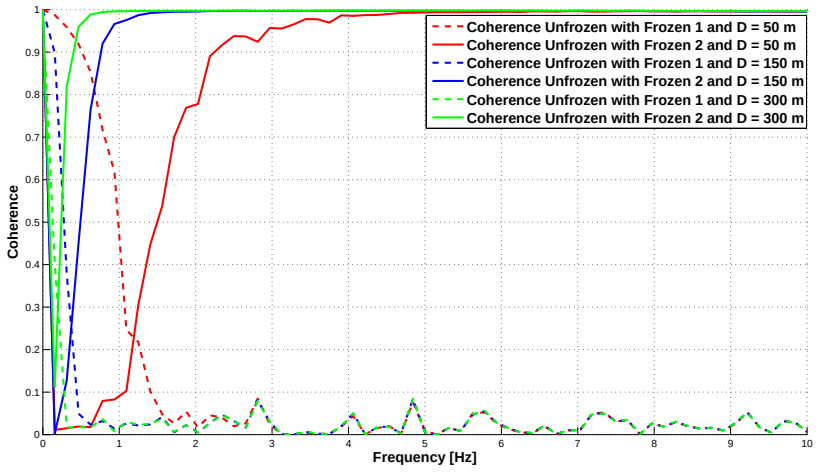

Figure 3.7: Comparison between three different unfrozen wind histories in terms of the longitudinal coherence, changing the parameter D

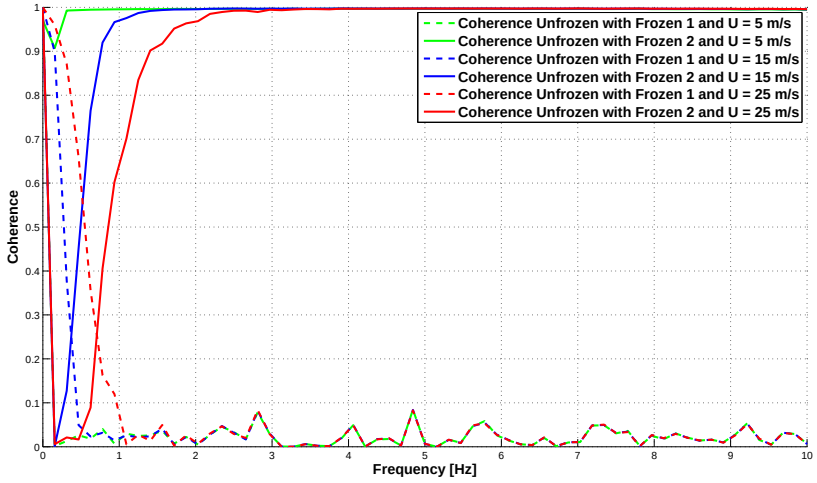

Figure 3.8: Comparison between three different unfrozen wind histories in terms of the longitudinal coherence, changing the parameter U_0

For consistency with previous works of DAST-Polimi the theory described in *Turbsim Manual* was employed as the base of the model. As we can see from reference [25], this code meets the requirements. Therefore a new code is written following articles [23], [26] and [25], also studying [24].

The greatest difference of this new turbulent wind generator with respect to the test model is that, in order to recreate a denser grid of values, it is necessary to consider the lateral coherence between one grid point and all the others. Therefore it is clear how this introduces others factors in the Eq. (3.27). Following Veers's work, reference [23] and [26], we can write a new equation for wind time series:

$$U(t) = \overline{U} + \sum_{j=1}^{N} (A_j sin\omega_j t + B_j cos\omega_j t) \tag{3.29}$$

where

$$A_j = sin\phi_j \sqrt{\frac{1}{2} S_j \Delta\omega} \tag{3.30}$$

and

$$B_j = cos\phi_j \sqrt{\frac{1}{2} S_j \Delta\omega} \tag{3.31}$$

Which it can be rewritten as

$$U(t) = \overline{U} + \mathfrak{F}^{-1} \sum_{j=1}^{N} (A_j + iB_j). \tag{3.32}$$

where $\mathfrak{F}^{-1}$ is the inverse Fourier transform.

This formulation of wind field does not yet take into account the coherence between one point and all the others, but only develops a more complete unrelated wind. This represents the base of the following formulation. We want to focus only on turbulent fluctuations, because this is the main aspect of a related wind field. For this purpose a new spectral matrix must be introduced, called **S**. The peculiarity of this matrix is that its diagonal terms are the power spectral densities (PSDs); instead, each off-diagonal term, S_{ij}, is the cross spectral density between points i and j (CSD). The magnitude of the cross spectrum between points i and j can be defined in terms of the PSDs and the coherence function, Coh_{ij}, as

$$|S_{ij}(n_m)| = Coh_{ij}(n_m, \Delta r_{ij}, U_{ij}) \sqrt{S_{ii}(n_m) S_{jj}(n_m)} \tag{3.33}$$

where the coherence is a function of frequency, n_m, distance between points i and j, Δr_{ij}, and mean wind speed, U_{ij}.

The N correlated time series are generated by linear combination of N independent, white-noise processes. In this case, **S** can be written as the product of a transformation matrix, **H**, and the transpose of its complex conjugate.

$$\mathbf{S} = \mathbf{H}(n_m)\mathbf{H}^{*^T}(n_m) \tag{3.34}$$

Physically, **H** is a transfer matrix from uncorrelated white noise to the correlated spectra of the wind at input points. It is a lower triangular matrix, and then it is completely defined by Eq.(3.34). The elements of **H** can be determined recursively:

$$\begin{aligned}
H_{11} &= S_{11}^{1/2} \\
H_{21} &= S_{21}/H_{11} \\
H_{22} &= (S_{22} - H_{21}^2)^{1/2} \\
H_{31} &= S_{31}/H_{11} \\
H_{32} &= (S_{32} - H_{31}H_{21}/H_{22} \\
&\vdots \\
H_{ii} &= (S_{ii} - \sum_{j=1}^{i-1} H_{ij}^2)^{1/2} \\
H_{ij} &= (S_{ij} - \sum_{k=1}^{j-1} H_{ik}H_{jk})/H_{jj}
\end{aligned}$$

Instead the independent, unit-magnitude, white noise inputs are contained in an $N \times N$ diagonal matrix **X** such that

$$X_{ij}(n) = \begin{cases} e^{i\theta_{jm}} & i = j \\ 0 & i \neq j \end{cases} \tag{3.36}$$

where θ_{jm} is a random phase associated to the j^{th} input point and m^{th} frequency component. To unfreeze the turbulence we must work on θ_{jm}. In fact, $e^{i\theta_{jm}}$ is considered equal to $cos\theta + isin\theta$. Therefore the Eq. (3.25) is applicable, switching from two frozen seeds to an unfrozen one. Defined this new phase, it is possible to compute the unfrozen turbulence fluctuations.

$$u(t) = \mathfrak{F}^{-1}(\mathbf{HX}) \tag{3.37}$$

Then the completed wind field can be written as

$$U_k(t) = \overline{U}_k + u(t)_k \qquad \text{where} \quad k = u, v, w \tag{3.38}$$

3.3 Unfrozen LiDAR Sensor

The frozen LiDAR simulator consists of five focuses and 101 detection points for each focus. For a frozen LiDAR this is not a problem, because a unique wind time

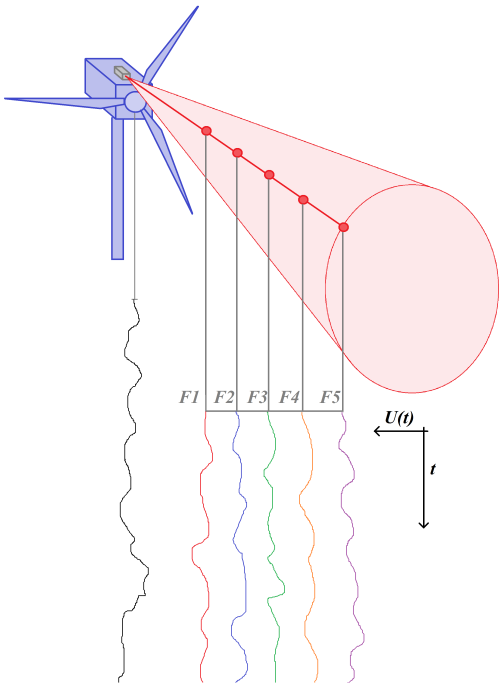

Figure 3.9: Sketch of LiDAR detection points. Only focus points are shown. For each focus is represented its wind time histories, that it is different from the others

series is sufficient as it is convertible to a wind spatial series, thanks to the Taylor Hypothesis. Regarding an *Unfrozen LiDAR* this procedure is not feasible, because the intent is to eliminate this hypothesis. Therefore we considered a simple wind time series that is seen by the turbine, and consequently we must unfreeze the wind field in the longitudinal direction, as Figure 3.9. This means generating 505 unfrozen wind time histories, one for each measurement point (the number of unfrozen wind time histories is given by the number of focuses and 101 detection points for each focus). Then the LiDAR takes the wind velocities from these histories as input, one for each distance of detection point to wind turbine.

It's important to notice that with this simulation strategy, the model that detects the exact wind speed is the frozen LiDAR, because it detects the exact wind history that hits the wind turbine. However, what is certain is that the two types of LiDAR provide two signals which differ a little, as it can be noticed in Figure 3.10.

It's useful for understanding the mechanisms of turbulence unfreezing to see Figures 3.11 and 3.12. In both figures the LiDAR output is plotted. Looking at Figure 3.11 and recalling that the first seed characterize the wind hitting the turbine, we notice that keeping it fixed and changing the second, we obtain very similar LiDAR outputs. This result means that the distance of the focal points is too low to raise the value of the decay , then the second seed has little influence on the final value of the wind. This

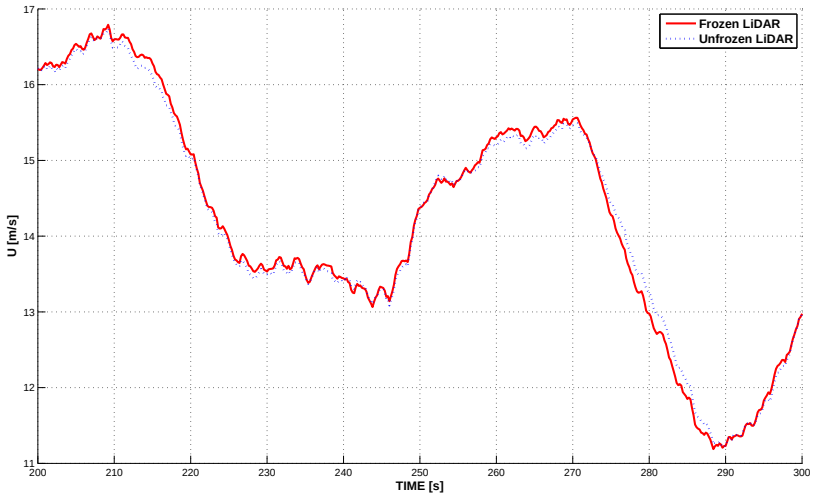

Figure 3.10: Comparison between Frozen and Unfrozen LiDAR for a wind speed equal to 15 m/s.

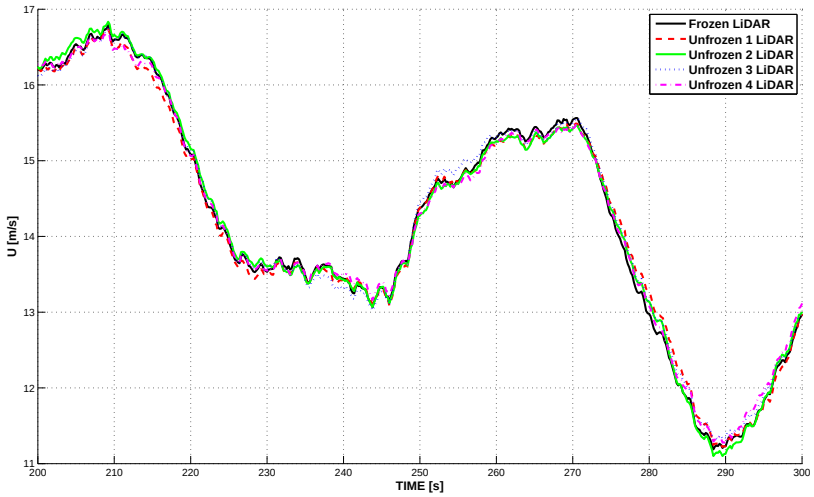

Figure 3.11: Five output detected by LiDAR is shown, one derived from frozen wind field and the others derived from unfrozen wind field. The characteristic of these simulations are that the first seed of turbulence is fixed while the second one is variable

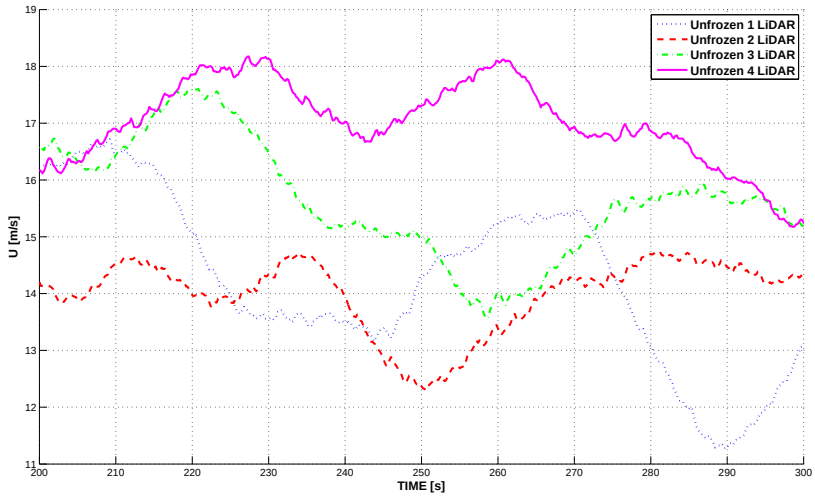

Figure 3.12: Four output detected by LiDAR is shown, all these derived from unfrozen wind field. The characteristic of these simulations are that the first seed of turbulence is variable while the second one is fixed

trend can be verified also in Figure 3.12. In fact, in this figure the LiDAR outputs are plotted. They are characterized by the second seed fixed while the first one is variable. The consequence of this simulation is that we obtain four different LiDAR signals, as if they were four different wind histories.

3.4 Implementation Aspects

The implementation was one of the crucial aspects of this work. In general there are two types of controller configurations, one with LiDAR on real time, and one with LiDAR simulation separated from Cp-Lambda simulation. Clearly the first choice implies a great memory saving because all simulations are on real time. Hence, there is no need to store a large amount of data because all the data computed by the LiDAR are used instantly and overwritten. This advantage has a cost, in fact the time simulation explodes. Contrariwise the second choice allows to reduce substantially the simulation time, because LiDAR simulation is computed separately from Cp-Lambda simulations and its output is stored in a physical memory. The consequence is an increase in required storage space. Given our resources it seemed convenient to prefer the second choice, because the increase of data storage is lower than the corresponding increase in time simulation that characterize the first choice.

Another implementation aspect that we had to deal with, relates to the use of unfrozen LiDAR. As described above, unfrozen LiDAR needs 505 unfrozen wind histories, one for each distance between detection points and the wind turbine. Therefore in

order to reduce both time simulation and data storage, it was developed a code that, in the first step, computes 505 unfrozen wind histories, but without saving anything. In the second step the code computes a linear interpolation, to find, for each wind grid, the value of speed for each pattern point. We want to remind that the pattern points are those that identify the LiDAR detection points, where the real LiDAR measures the wind speed. After this the code saves only the value of linear interpolation, then twelve values for each time step and for each longitudinal displacement from the turbine. The data that is stored is used as input of unfrozen LiDAR, the output is one value of wind speed like for the frozen LiDAR. For this procedure it is highly recommended the use of PC with parallel processors, at least eight, which allow the programming of code that can exploit them simultaneously and reduce simulation time considerably.

Chapter 4

Applications

The purpose of this section is to show the differences between three different control systems, and in particular the possible improvements in the use of the unfrozen LiDAR simulator against the frozen one. The control strategies, that we take into account, are the LQR-Integral controller, considered as a reference, and the others are the NHLQR and the RHC, i.e. two predictive control strategies. An exhaustive description of the main characteristics of these controllers can be seen in chapter 2. In particular it is useful to emphasize that all the simulations and their results here reported comply with the International Standard, reference [33]. This means that all results that we report here are obtained by an average between at least four simulations, corresponding to four different turbulent seeds. Therefore to underline the goodness of employing a predictive control, four wind time histories have been considered. The goal of this intention is to report a correct data from the statistical point of view, as required by International Standard.

The simulation strategy to explore whether the unfrozen LiDAR can improve the prediction of the incoming wind is also based on the average between four different wind histories. Nevertheless, in order to unfreeze the wind field, a second random phase is necessary. Hence, four additional simulations are required for each wind history, only for the purpose to obtain a simulation with the unfrozen LiDAR which is correct under a statistical point of view.

As described above we consider four wind time histories, provided by TurbSim, that the wind turbine sees one at a time, as is shown in Figure 4.1. Therefore we use the output of TurbSim as input of Cp-Lambda. Instead the input of the predictive control is provided by unfrozen and frozen off-line LiDAR simulators. In case we want to define the unfrozen wind signal, we must unfreeze the flow field in front of the turbine. This means that we need to use a program that allows to create an unfrozen turbulent wind field, described in chapter 3, where the first seed, that characterizes the unfrozen wind, is defined by one of the four wind time histories that we consider as the wind seen by the turbine. To fulfill the requirements of the International Standard, 16 unfrozen LiDAR simulations are computed, four for each frozen wind history. The consequence is that the results of unfrozen simulations are obtained by two averages.

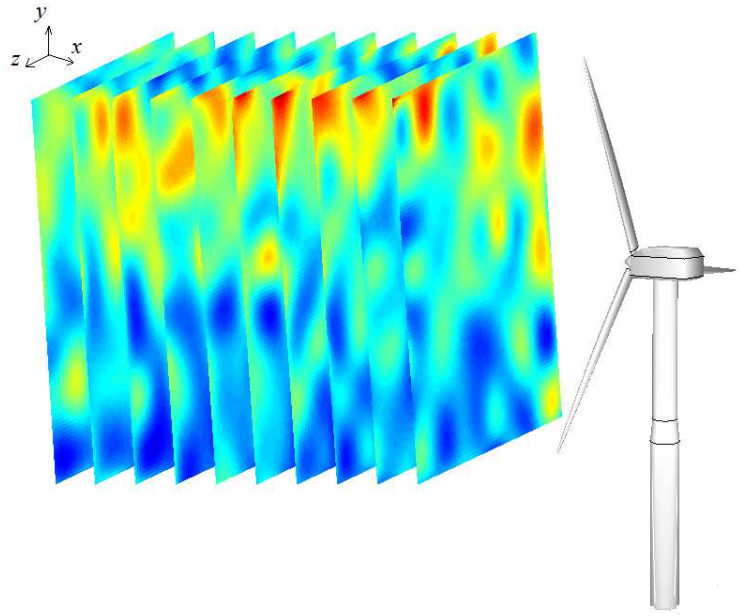

Figure 4.1: Sketch of wind field in front of the turbine

The first average is between four different simulations, characterized by the first (fixed) seed and the second (variable) seed, then four different values of second (variable) seed are considered. This operation is computed by varying also the first seed. Finally there is the second average between the four simulations obtained from the first average.

In all graphs reported here there are 5 curves. One of these represents the results obtained with the reference controller, LQR-Integral. Two of these represent the NHLQR predictive controller, one using the frozen LiDAR and one using the unfrozen LiDAR. The last two curves represent the RHC predictive controller, and as for NHLQR simulations one of these curves is computed using the frozen LiDAR and one using the unfrozen LiDAR.

It is also useful to say a few words about the parameters used to make the comparison. In particular the M_y tower base bending moment, Figure 1.9, standard deviation of rotor speed and standard deviation of power are selected. It is clear that it should be possible to select many other parameters for a comparison between different control systems, since there are many other loads acting on the wind turbine structure. But we consider only the fatigue characterized by the load acting on the fore-aft of tower because it is a parameter that we have the ability to control by the control system. This because one terms of the states vector of the control technique is represented by the fore-aft velocity. Instead it seemed natural to choose the other two parameters, because the standard deviation of the rotor speed is a typical value that is used to compare

different control strategies, and because it is the most important value that represents how a machine is nervous under the control law which regulate it. On the contrary the standard deviation of power is the best index of the power quality.

For completeness this simulations system is proposed for two different wind turbines. The first turbine considered is the *Kangwon Turbine* while the second one is the *Innwind Turbine*. All main characteristics of these machines are discussed in next section. In particular it is useful to emphasize how they represent two real machines with different rotor sizes. For this reason the graphs reported here are all dimensionless because the data design are covered by industrial secrecy.

4.1 Machine Models

As described above all the simulations reported in this work are obtained using the virtual models of two real machines: *Kangwon Turbine* and *Innwind Trubine*. The designs of these two wind turbines are covered by industrial secrecy then only their main characteristics are shown in this section.

- *Kangwon Turbine:* The Kangwon Turbine is a 3.0 MW machine designed by the Kangwon National University [34]. It features a rotor diameter in excess of 93 m, a tower height of about 77 m, a drive-train with a reduction ratio of about 90. This machine is certified as IEC class A, and its operating wind speed envelope goes from 3 to 25 m/sec, with a region $II\frac{1}{2}$ extending from 9 m/sec to the rated wind speed of 11.5 m/sec. The standard operating rotor speed in region *III* is 15 rpm.

Table 4.1: Main characteristics of Kangwon Turbine

Parameter	Value
Rotor diameter	93 m
Tower height	77 m
Hub height	80 m
Cut-in speed	3 m/s
Cut-out speed	25 m/s

- *The Innwind Turbine:* The Innwind Turbine is a 10.0 MW machine designed by the European consortium that comprises of leading Industrial Partners and Research Establishments [35]. It features a rotor diameter of about 180 m, a tower height of about 115 m. This machine is certified as IEC class 1A, and its operating wind speed envelope goes from 4 to 25 m/sec, with rated wind speed of about 11 m/s. The maximum rotor speed is 10 rpm.

Table 4.2: Main characteristics of Innwind Turbine

Parameter	Value
Rotor diameter	180 m
Tower height	115 m
Hub height	120 m
Cut-in speed	4 m/s
Cut-out speed	25 m/s

4.2 Results

The International Standard requires reliable results from the statistical point of view to certificate whatever controller or amendment to the design of a wind turbine. This means that we consider for all results reported here an average between four different simulations. These four simulations are represented by four different wind histories that the wind turbine sees. The consequence is that the first seed of whatever unfrozen wind is fixed by the corresponding main wind history (one among the four chosen). To fulfill the International Standard a simulation with unfrozen LiDAR requires another four sets of wind histories for the statistical evaluation of the second seed. Therefore the results of simulations with unfrozen LiDAR is averaged between 16 different simulations, four simulations for each main wind histories. Whereby we consider three different controllers, one in feed-back and the others in feed-forward with frozen and unfrozen LiDAR, the amount of CP-Lambda simulations are shown in Table 4.3.

Table 4.3: Summary scheme of number simulations for each control strategy

Controller	LiDAR simulator	Simulations	Description
LQR-Integral	//	4	One for each main wind histories
NHLQR	Frozen	4	One for each main wind histories
NHLQR	Unfrozen	16	Four for each main wind histories
RHC	Frozen	4	One for each main wind histories
RHC	Unfrozen	16	Four for each main wind histories

Clearly the four main wind histories considered are four turbulent winds, with a turbulent intensity equal to 16%, type of turbulence A. This is the highest turbulent intensity, as required by International Standard. In particular all wind operating ranges of the turbines are considered, and Kaimal spectrum is chosen as a spectrum of turbulence. The other parameters of section *Meteorological Boundary Conditions* of input file of TurbSim are set to default, [25].

As described above three parameters are chosen to compare to the simulations results between LQR-Integral and NHLQR and RHC controllers:

- *Fatigue:* The fatigue considered is referred to the load, M_y tower base bending moment. Clearly there are many other loads that act on the wind turbine. Nevertheless this load is chosen because the controllers considered have the velocity of the fore-aft of tower, $\dot{d}$, as a parameter of the state array. Therefore it seemed natural to choose this type of load. This value is made non-dimensional with a reference value because in order to preserving industrial secrecy.

- *Standard Deviation of Rotor Speed:* This is a typical parameter that it is used to verify the goodness of the controllers considered. Another reason for the choice of this parameter is because it can be a good indicator of the operation of the machine. In particular if this has a value too high then it may indicate the probability of the shutdown of the machine during the simulation. This value is made non-dimensional with the maximum value of rotor speed detected during simulation.

- *Standard Deviation of Power:* Clearly between the chosen parameters could not miss one related to power. This because we are interested in a good *Power Quality*. Then the standard deviation of Power is chosen. This value is made non-dimensional with the maximum value of power produced during simulation.

4.2.1 3MW Kangwon Turbine Results

The results reported in this subsection are referred to the Kangwon Turbine. The order in which they are listed is the same as described above. It is important to emphasize that the Region II$\frac{1}{2}$ extends from 9 m/s to 11.5 m/s, in this range of velocity it is possible to obtain performance values of predictive controllers very similar to LQR-Integral. Instead the simulations at wind speed 3 m/s and 25 m/s are critical, because the turbulent intensity can be lead to lower speed than U_{cut-in} or greater than $U_{cut-out}$. In particular in Region II the controllers are limited by the fixed pitch strategy. Each figure in this section shows a pair of graphs, referring to same results. In all cases, the first plot is made non-dimensional with a reference value (not explicit, due to industrial copyright), instead the second plot is made non-dimensional with LQR-Integral.

In the first figure, Figure 4.2, the trends of fatigue for each control strategy are shown. It can be noticed that the solid red line, that represents the LQR-Integral simulations, has performance values higher than NHLQR and RHC with both LiDAR simulators. This means that in terms of the values of loads acting on the wind turbine, the LQR-Integral imposes the highest values between all control strategies considered, all over the entire speed range. Besides that we are interested in the comparison between the Unfrozen LiDAR simulator and the Frozen one. The results reported here are clear, for the NHLQR controller there aren't any differences between two simulations (Unfrozen and Frozen one). In case that we consider the RHC controller there is a very low difference, that does not justify the use of a simulator rather than another. In particular it is important to emphasize that the results of the RHC controller are the best

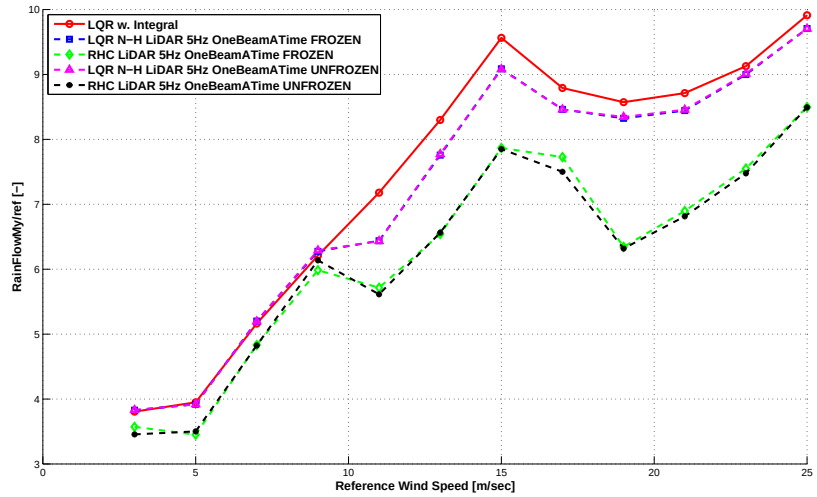

(a) *Made non-dimensional with reference value*

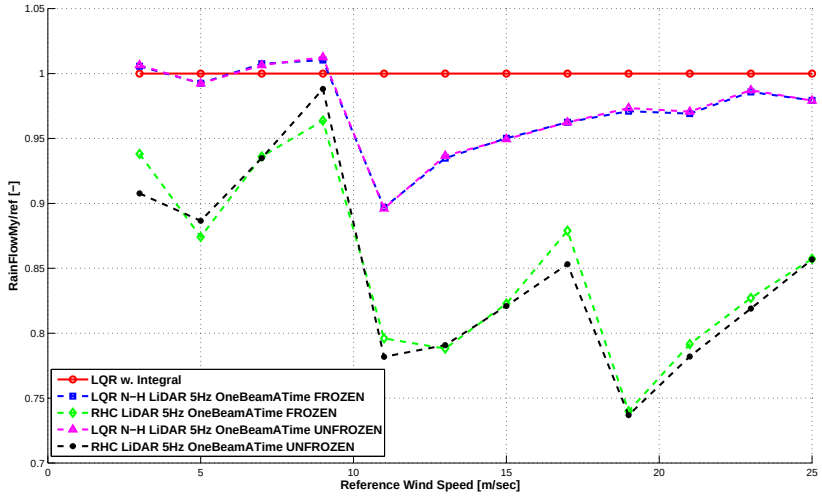

(b) *Made non-dimensional with LQR-Integral value*

Figure 4.2: Kangwon Turbine Results: Value of fatigue along the operating speed range of the machine, made non-dimensional with reference value (not reportable)

here reported. In fact, the nature of NHLQR controller is to improve the performance of the basic LQR-Integral, but with a computational cost roughly 1000 times lower than RHC controller, the consequence is that the controller performance of NHLQR is lower than RHC. Another behavior that can be noticed is the very close trend between the NHLQR and LQR-Integral controllers in Region II; RHC controller also has a performance close enough to the other controllers in that region. This underlines the difficulties of predictive controls at certain speeds.

In Figure 4.3 are shown the trends of standard deviation of the rotor speed. It can be noticed that in Region III (for $U > 11m/s$) the trends of NHLQR and RHC controllers are very close and at the same time they are very low in comparison to LQR-Integral controller. In terms of the rotor speed the critical region for the predictive controllers is the Region $II\frac{1}{2}$, in fact, both these controllers have a value of standard deviation very similar to LQR-Integral values. Besides that it can be seen that the values of RHC for the simulation at speed 3 m/s are too high in comparison to the other controllers. This bad performance is related to the shutdown of the machine.

In Figure 4.4 are shown the trends of the standard deviation of power. Once again it can be noticed that LQR-Integral controller performances are higher than the predictive control strategies. It is also important to emphasize that the differences between the Unfrozen LiDAR simulator and the Frozen one are rather low. In Region II if we consider the RHC controller there are values of standard deviation of power very low in comparison to LQR-Integral, this means a better behavior of the machine at low speed. In region III the values seem very close, but this is not true, in fact in terms of percentage the improvements are remarkable, see Figure 4.4(b).

In conclusion for the Kangwon Turbine the predictive controls developed provide better performance than a basic LQR-Integral controller. The differences between simulations with Unfrozen LiDAR sensor and Frozen LiDAR sensor are not significant.

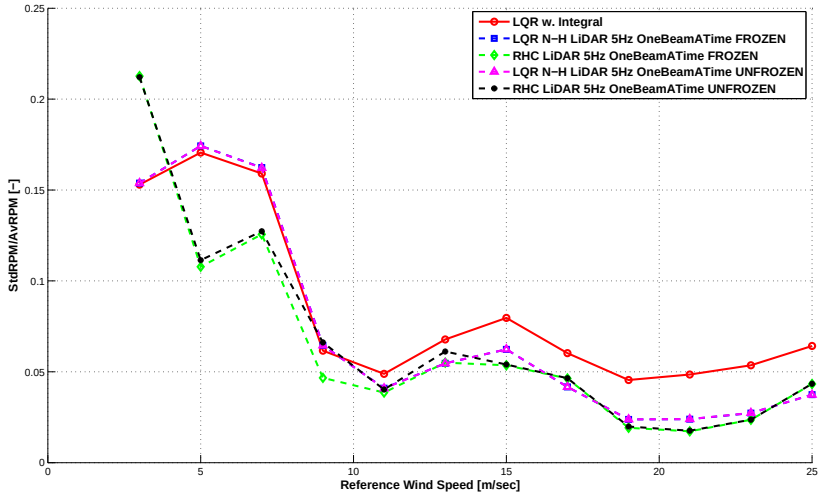

(a) *Made non-dimensional with reference value*

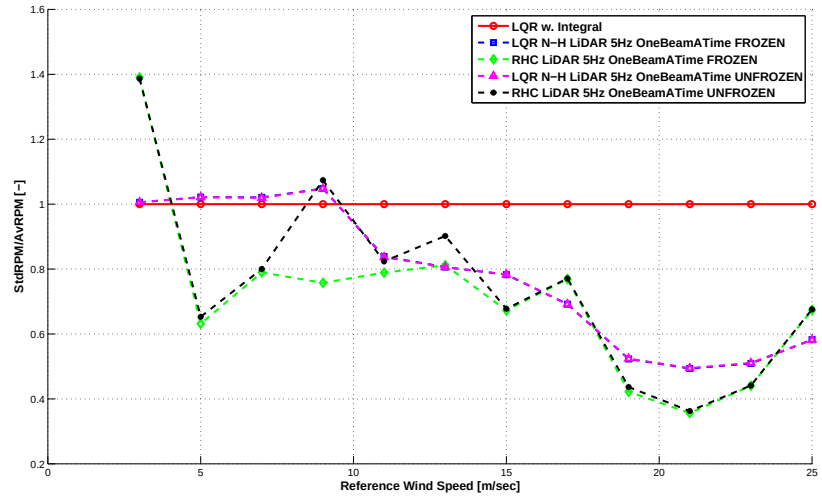

(b) *Made non-dimensional with LQR-Integral value*

Figure 4.3: Kangwon Turbine Results: Value of standard deviation of the rotor speed along the operating speed range of the machine, made non-dimensional with reference value (not reportable)

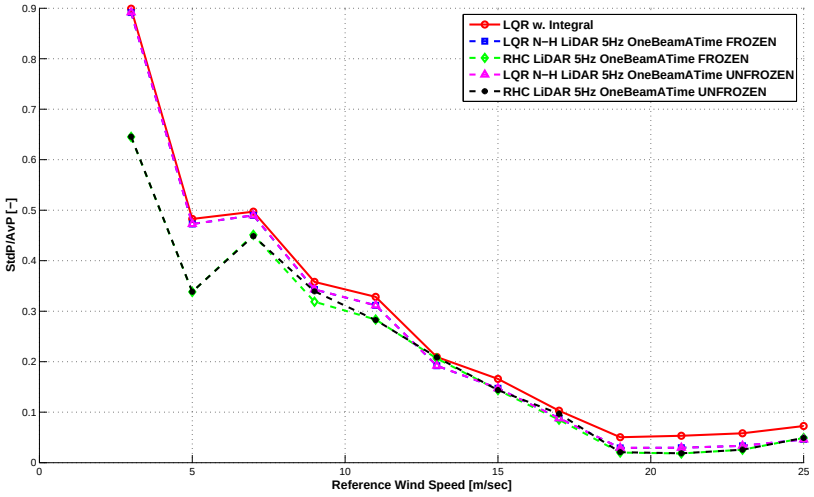

(a) *Made non-dimensional with reference value*

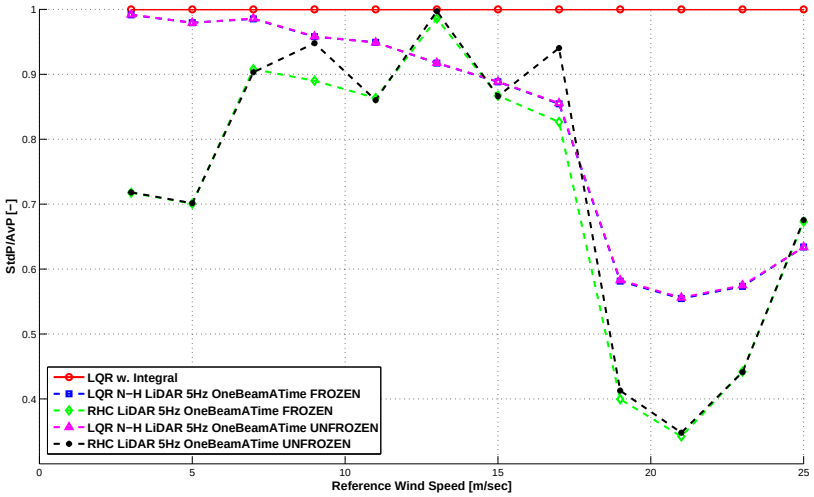

(b) *Made non-dimensional with LQR-Integral value*

Figure 4.4: Kangwon Turbine Results: Value of standard deviation of the power along the operating speed range of the machine, made non-dimensional with reference value (not reportable)

4.2.2 10MW Innwind Turbine Results

The results reported in this subsection are referred to the Innwind Turbine. The same observations made for the other machine can also be done in this case. Important to emphasize that the simulations at speed 3 m/s are excluded, because that wind is lower than U_{cut-in}. Each figure in this section shows a pair of graphs, referring to same results. In all cases, the first plot is made non-dimensional with a reference value (not explicit, due to industrial copyright), instead the second plot is made non-dimensional with LQR-Integral.

In Figure 4.5 it can be noticed that the red solid line that represents the LQR simulations shows bad performance in comparison to the others. As in the case reported before also for this turbine the best controller is represented by RHC. It can be seen that also in this case the critical region is the Region II. In particular for NHLQR also the Region II$\frac{1}{2}$ is critical. Instead the differences between simulations with different LiDAR strategy are very low, then also in this case the performance of the two LiDARs is very close.

In Figure 4.6 it can be noticed immediately that the values of standard deviation of rotor speed of simulations with NHLQR controller in Region III are the worst. This behavior depends on gains scheduling of this controller. In fact, it was made a compromise choice, because with some values of the controller weights the value of standard deviation of rotor speed has improved but at the same time the value of the fatigue or standard deviation of power have worsened. In fact, tuning some weight values we tried to improve three different performance indexes, such us Fatigue, standard deviation of rotor speed and standard deviation of power. Therefore the results reported here derive from the best choice of weight that we have done. It is possible that there are others controller weights that give better results. It is important to emphasize that the values of the standard deviation of the rotor speed of NHLQR control simulations in Region III are not so disappointing. In fact, these results, in comparison to those obtained with Kangowon Turbine, show a considerable improvement, the values of NHLQR simulations of Innwind Turbine amounted to 2% while the values of NHLQR simulations of Kangowon Turbine amounted to 3%. Finally it can be seen that in the region II the performance of predictive controls, and in particular of RHC, are better than LQR-Integral controller.

In Figure 4.7 it can be noticed that the predictive controls lead to better power quality than the basic controller. The curves that represent the predictive controls are below the red solid line. In terms of standard deviation of power, simulations on both the Innwind Turbine and Kangowon Turbine, have demonstrated that the predictive controls are definitely better performing than LQR-Integral control.

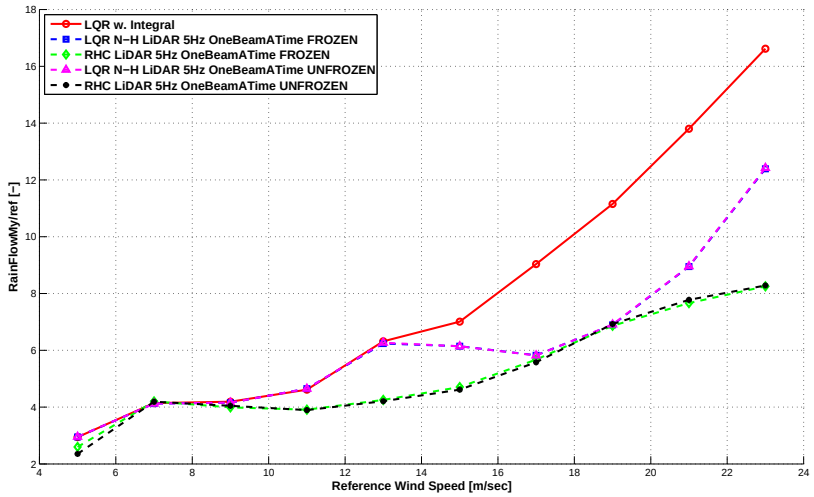

(a) *Made non-dimensional with reference value*

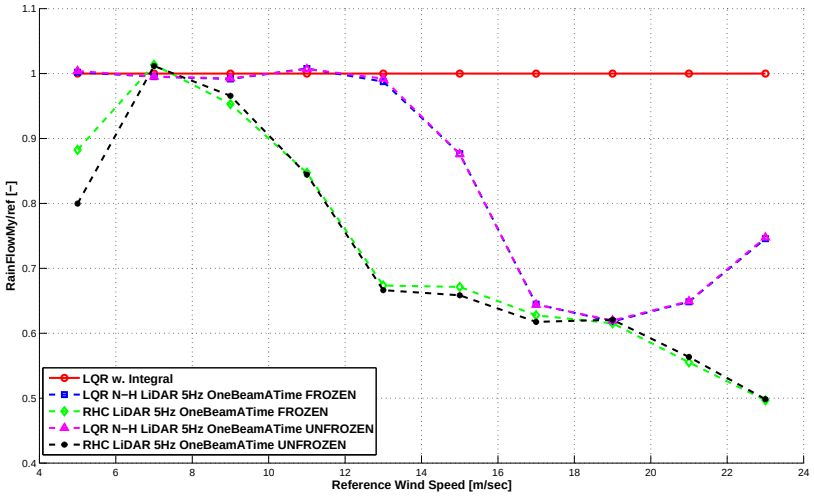

(b) *Made non-dimensional with LQR-Integral value*

Figure 4.5: Innwind Turbine Results: Value of fatigue along the operating speed range of the machine, made non-dimensional with reference value (not reportable)

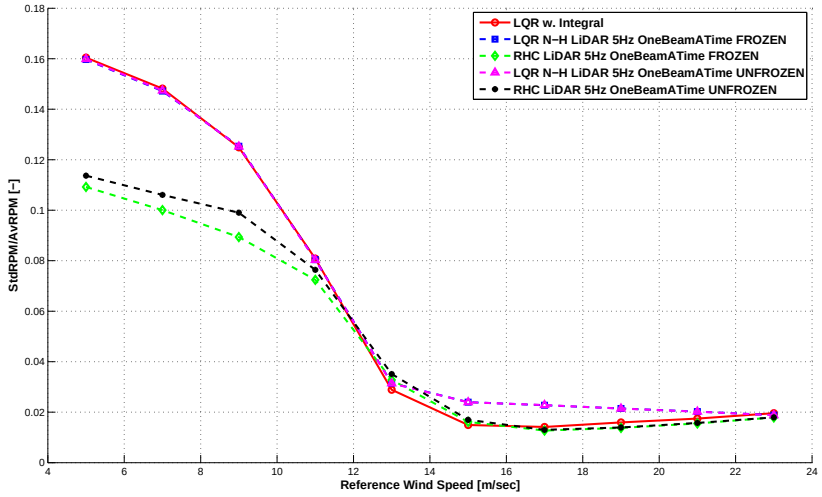

(a) *Made non-dimensional with reference value*

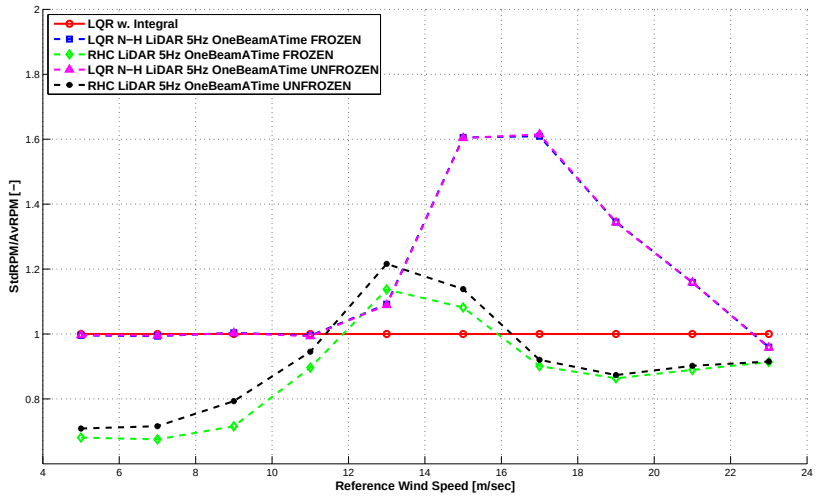

(b) *Made non-dimensional with LQR-Integral value*

Figure 4.6: Innwind Turbine Results: Value of standard deviation of the rotor speed along the operating speed range of the machine, made non-dimensional with reference value (not reportable)

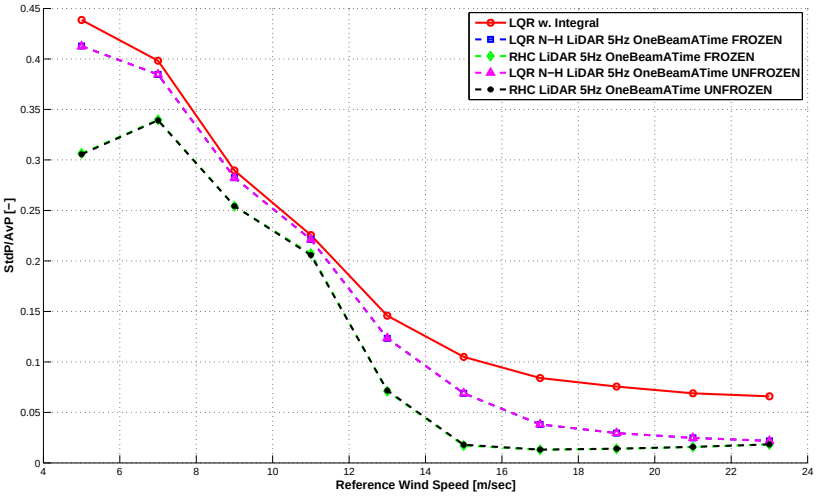

(a) *Made non-dimensional with reference value*

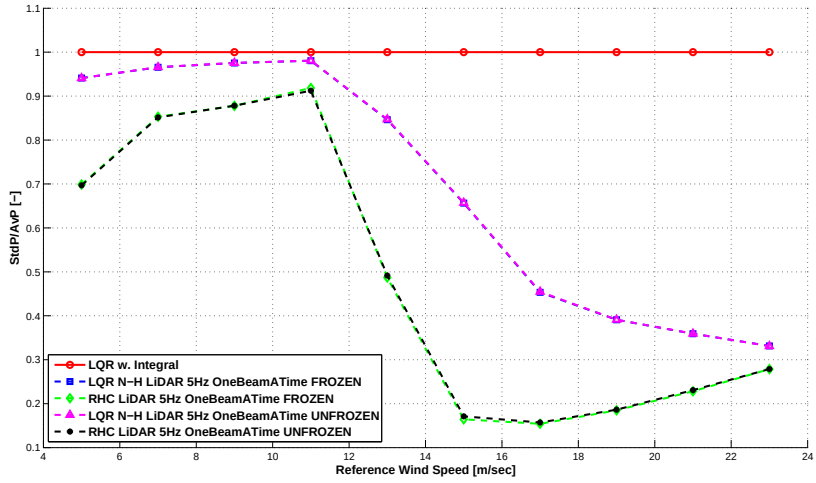

(b) *Made non-dimensional with LQR-Integral value*

Figure 4.7: Innwind Turbine Results: Value of standard deviation of the power along the operating speed range of the machine, made non-dimensional with reference value (not reportable)

Chapter 5

Conclusion

The purpose of this work was to analyze the possibility of improving the use of *Unfrozen LiDAR technology* as a sensor to provide the feed-forward information to the predictive controller. It was also verified the remarkable improvements obtained thanks to the use of the predictive control strategy against a basic feed-back control strategy, such as LQR-Integral.

As described in chapter 3, the unfrozen LiDAR is based on the theory developed by Kirstensen, i.e. a mathematical model that allows to unfreeze the turbulence having as input the time average velocity of the wind field and the displacement between the point to unfreeze and the reference point. Initially this model was not related to any LiDAR sensor, in fact, it was developed in the Seventies of the last century, then largely verified. It is a semi-empirical model and it is strictly related to the chosen turbulence model. Then the Kirstensen model also depends on the value of turbulent intensity, on the type of spectrum and on the value of turbulent integral length scale. The mathematical model provides a coherence value as a function of frequency, and this value is useful to determine the transition from one wind history to another, generating a third wind time history that is called *Unfrozen*. Recently many researchers have tried to improve the available Frozen LiDAR sensor with this mathematical model, transforming it into the Unfrozen LiDAR. This is because the need to provide a better information to predictive controller has arisen. It's clear that if the controller may have a better incoming wind information, then the performance can be improved. This is a theoretical idea, in fact, this work is focused on understanding the possible improvement that the unfrozen LiDAR involve, and most in general to emphasize the improvements of predictive control law.

The remarkable improvements of the predictive control law obtained in the previous work by the DAST-Polimi are confirmed. This trend is verified with two real turbines with different rotor size and energy production. It was understood, therefore, that the use of predictive controls can significantly decrease the costs involving the production and maintenance of the machines. This is because, as it can be noticed in the graphs that represent the simulations results in chapter four, the fatigue, which is referred to the loads acting on tower fore-aft, is considerably reduced compared to the

basic LQR-Integral controller. The other comparison parameter is the standard deviation of rotor speed, in this case the trends of all controllers considered have a very low value of standard deviation, then it can be possible to consider these control strategies as suitable. Finally the standard deviation of power is taken into account, in this case it can be noticed how the predictive control strategy provides a more smooth trend, therefore with this behavior better power quality than with LQR-Integral is obtained. Regarding the simulations case with the use of Unfrozen LiDAR sensor to provide the incoming wind information, the results obtained are also very remarkable. In fact, the trends of the results are better than simulations results of LQR-Integral controller. However, better results were expected even with respect to frozen predictive control. This has not happened, the results, which as mentioned above are averaged between four different simulations to meet the requirements of International Standard, are almost identical to results obtained by frozen simulations. This behavior depends on the displacements of each focus from the turbine. As described above these distances are comparable to the turbulent integral length scale. The consequence of this characteristic of the focuses of Unfrozen LiDAR leads to a value of decay which is very low, as defined in chapter 3, then a decay parameter that is not high enough. This behavior can be seen also looking at the output of LiDAR, in fact, the signals, provided by Frozen and Unfrozen LiDAR, are very close. Furthermore, it can also be emphasized the fact that the small variations that exist between different models of LiDAR, passing through the controller, could in principle smooth even those small differences, because the controller basically acts as a filter.

In conclusion the predictive control strategies are one of the better ways to reduce the cost of the wind turbine. Instead the adjustment of the Frozen LiDAR sensor by accounting for the mathematical model developed by Kirstensen for Unfrozen LiDAR sensor does not seem to give advantages against the original LiDAR implementation.

5.1 Future Works

Nowadays a development of the unfrozen LiDAR is strictly related to the experimental campaigns. The results of virtual simulations with Unfrozen LiDAR are almost unchanged when compared to the Frozen LiDAR, then it would seem a useless technology. Nevertheless there is the possibility that the experimental campaigns can improve the empirical-mathematical model that characterized the Unfrozen LiDAR.

It is useful to emphasize that in general the LiDAR sensor has a huge potential. In fact, nowadays, the LiDAR sensor is installed as a device for the predictive control of collective pitch strategy. In the future it can be introduced as part of the new idea of predictive control, that is, when individual pitch or distributed control is used. To do that the averages computed by LiDAR sensor must be changed. In fact the LiDAR sensor as developed today is not useful to provide an incoming wind information in the case of the hypothetical individual pitch predictive control, because it provides only one value of wind velocity for each time instant. Therefore to develop a sensor useful

for individual pitch predictive control the strategy to detect the wind speed, inside the LIDAR, must be changed. Then, the detection pattern and the output of the LiDAR sensor must change accordingly. We can imagine that a useful information for this new predictive control should be the horizontal wind shear and vertical wind shear.

Another improvement in this field can be to improve the gains scheduling of the predictive controller. One of the main causes of time-losses in this work was the need to set the weights of the matrices of control, because we must handle a multi-input vector. Therefore we imagine a possible optimization system to improve the time taken in the choice of the weights of the gains matrices. the choice of the weight is a very general issue concerning a great many model based controllers.

Bibliography

[1] *Global Wind Statistics 2012*, GWEC (Global Wind Energy Council)

[2] Justin Wilkes, Jacopo Moccia. *Wind in Power 2012 European Statistics*, EWEA (European Wind Energy Association)

[3] www.iea.org, IEA (International Energy Agency)

[4] Carlo E.D. Riboldi. *Advanced Control Laws For Variable-Speed Wind Turbines and Supporting Enabling Technolgies*. PhD thesis, Dipartimento di Ingegneria Aerospaziale, Politecnico di Milano, Milano, Italy, 2012

[5] Pietro Pizzinelli. *LiDAR-Enabled Predictive Control of Wind Turbines*. Master thesis, Dipartimento di Elettronica e Informazione, Politecnico di Milano, Milano, Italy, 2012

[6] Giulio Giansiracusa. *Tecniche di Controllo Predittivo per Aerogeneratori con Ausilio di Strumentazione LiDAR*. Master thesis, Dipartimento di Ingegneria Aerospaziale, Politecnico di Milano, Milano, Italy, 2011

[7] Carlo L. Bottasso. *Progetto di Generatori Eolici - Wind Turbine Control*. Master Course of the Department of Aerospace Sciences and Technologies of Politecnico di Milano, 2011

[8] Carlo L. Bottasso. *Progetto di Generatori Eolici - Wind Turbine Modeling*. Master Course of the Department of Aerospace Sciences and Technologies of Politecnico di Milano, 2011

[9] David Schlipf. *LiDAR Assisted Control of Wind Turbines*. Struttgart Wind Energy. Universitat Stuttgart.

[10] David Schlipf, Stefan Kapp, Jan Anger, Oliver Bischoff, Martin Hofsäß, Andreas Rettenmeier and Martin Kühn. *Prospects of Optimization of Energy Production by LiDAR Assisted Control of Wind Turbines*.

[11] Ervin Bossanyi. *Un-Freezing the turbulence: improved wind field modelling for investigation Lidar assisted wind turbine control*. GL Garrad Hassan

[12] Stephen B. Pope. *Turbulent Flows*. Cornell University. Cambridge University Press.

[13] L. Kristensen. *On Longitudinal Spectral Coherence*. Riso National Laboratory, DK-4000 Roskilde, Denmark.

[14] J.L. Lumley, H.A. Panofsky. *The structure of atmospheric turbulence*, *Interscience Monographs and texts in Physics and Astronimy*, Jhon Wiley and Sons.

[15] C.F. Ropelewski, H. Tennekes, and H.A. Panofsky. *Horizontal Coherence of wind fluctuations*. The Pennsylvania State University.

[16] A.G. Davenport. *The spectrum of Horizontal Gustiness Near the Ground in High Winds*, *Quarterly Journal of the Royal Meteorology Society* Volume 87, Issue 372, pages 194-211, April 1961

[17] J.C. Kaimal, J.C. Wyngaard, Y. Izumi and O.R. Coté. *Spectral Characteristics of Surface Layer Turbulence*, *Quarterly Journal of the Royal Meteorology Society* Volume 98, pages 563-589, February 1972.

[18] T. Burton, N. Jenkins, D. Sharpe and E. Bossanyi. *Wind Energy Handbook, Second Edition*. WILEY.

[19] H.A. Panofsky and T. Mizuno. *Horizontal Coherence and Pasquill's Beta*. Dept. of meteorology, The Pennsylvania State University.

[20] R.A. Pielke and H.A. Panofsky. *Turbulence Characteristics Along Several Towers*. Dept. of meteorology, College of Earth and Mineral Sciences, Pennsylvania State University.

[21] C.F. Ropelewski, H. Tennekes and H.A. Panofsky. *Horizontal Coherence of wind Fluctuations*. Pennsylvania State University.

[22] S.G. Perry, J.M.Norman, H.A. Panofsky and J.D. Martsolf. *Horizontal Coherence Decay Near large Mesoscale Variations in Topography*. Pennsylvania State University.

[23] P.S. Veers. *Three-Dimensional Wind Simulation*. Sandia Report. Sandia National Laboratories

[24] Jakob Mann. *Wind Field Simulation*. Danish Maritime Institute.

[25] B.J. Jonkoman, L. Kilcher. *TurbSim User's Guide: Version 1.06.00*. Technical Report. Nation Renewable Energy Laboratory.

[26] P.S. Veers. *Modeling Stochastic Wind Loads on Vertical Axis Wind Turbines*. SANDIA Report. Sandia National Laboratories.

[27] C.L. Bottasso, A. Croce, B. Savini, W. Sirchi, and L. Trainelli. *Aeroservo-elastic modeling and control of wind turbines using finite element multibody procedures*. Multibody System Dynamics, 16(3):291-308, 2006

[28] O.A. Bauchau, C.L. Bottasso, and Y.G. Nikishkov. *Modeling rotorcraft dynamics with finite element multibody procedures*. Mathematics and Computer Modeling, 33:1113-1137, 2001.

[29] E. Bossanyi. *Bladed for Windows theory manual*. Garrad Hassan, Bristol, UK, 1999.

[30] B. Jonkman and M. Buhl. *FAST User's Guide*. National Renewable Energy Laboratory (NREL), Golden, CO, August 2005.

[31] K. Stol and G. Bir. *SymDyn User's Guide*. National Renewable Energy Laboratory (NREL), Golden, CO, 2003.

[32] C.L. Bottasso e A. Croce. *Advanced Control Laws for Variable-Speed Wind Turbines and Supporting Enabling Technologies*, Scientific Report DIA-SR 09-01, Dipartimento di Ingegneria Aerospaziale, Politecnico di Milano, Milano, Italy, January 2009

[33] *Guideline for the Certification of Wind Turbines*, Rules and Guidelines Industrial Service IV. Germanischer Lloyd

[34] Kangwon National University. 1 Kangwondaehak-gil, Chuncheon-si, Gangwon-do, 200-701 Republic of Korea

[35] http://www.innwind.eu/